© 2020. Published by The Company of Biologists Ltd | Journal of Cell Science (2021) 134, jcs241752. doi:10.1242/jcs.241752

RESEARCH ARTICLE

SPECIAL ISSUE: CELL BIOLOGY OF HOST–PATHOGEN INTERACTIONS

Convergent Met and voltage-gated Ca^{2+} channel signaling drives hypermigration of *Toxoplasma*-infected dendritic cells

Einar B. Ólafsson[1], Arne L. ten Hoeve[1], Xiaoze Li-Wang[1], Linda Westermark[1], Manuel Varas-Godoy[2] and Antonio Barragan[1,*]

ABSTRACT

Ras–Erk MAPK signaling controls many of the principal pathways involved in metazoan cell motility, drives metastasis of multiple cancer types and is targeted in chemotherapy. However, its putative roles in immune cell functions or in infections have remained elusive. Here, using primary dendritic cells (DCs) in an infection model with the protozoan *Toxoplasma gondii*, we show that two pathways activated by infection converge on Ras–Erk MAPK signaling to promote migration of parasitized DCs. We report that signaling through the receptor tyrosine kinase Met (also known as HGF receptor) contributes to *T. gondii*-induced DC hypermotility. Furthermore, voltage-gated Ca^{2+} channel (VGCC, subtype $Ca_V1.3$) signaling impacted the migratory activation of DCs via calmodulin–calmodulin kinase II. We show that convergent VGCC signaling and Met signaling activate the GTPase Ras to drive Erk1 and Erk2 (also known as MAPK3 and MAPK1, respectively) phosphorylation and hypermotility of *T. gondii*-infected DCs. The data provide a molecular basis for the hypermigratory mesenchymal-to-amoeboid transition (MAT) of parasitized DCs. This emerging concept suggests that parasitized DCs acquire metastasis-like migratory properties that promote infection-related dissemination.

KEY WORDS: Receptor tyrosine kinase, Ca^{2+} signaling, Leukocyte motility, Amoeboid migration, Apicomplexa

INTRODUCTION

The mitogen-activated protein kinase (MAPK) Ras–Erk (used here to refer to Erk1 and Erk2; also known as MAPK3 and MAPK1, respectively) signaling axis plays important roles in cell migration, cell proliferation and survival, and cancer metastasis (Eblen, 2018). Ras GTPases function as molecular switches by cycling between an inactive and active state. Their function in cell motility is linked to their localization to the plasma membrane, which is mediated by farnesylation (Cox et al., 1992). At the plasma membrane, Ras is locally activated by guanine-nucleotide-exchange factors (GEFs). In turn, Ras activates the Raf–Mek–Erk signaling cascade, which regulates cell migration (Chernyavsky et al., 2005; Shi et al., 2019). When Ras is in proximity to the cell membrane, its activation can be mediated by diverse mechanisms, including receptor tyrosine kinase (RTK) signaling, integrin activation and Ca^{2+} influx (Giehl et al., 2000; Rosen et al., 1994; Schlaepfer et al., 1994).

In cancer cells, the RTK Met (also termed c-Met, hepatocyte growth factor receptor or HGFR) promotes cell migration and metastasis upon binding its ligand, hepatocyte growth factor (Hgf, scatter factor or SF) (Webb et al., 1998). Activated Met recruits RasGEFs, which locally activate Ras, leading to Erk phosphorylation and cell motility (Hartmann et al., 1994; Wang et al., 2002). Additionally, voltage-gated Ca^{2+} channels (VGCCs) mediate Ca^{2+} influx, which activates Ca^{2+}-sensing proteins locally at the plasma membrane (Dolmetsch et al., 2001; Rosen et al., 1994). In the context of cell migration, Ca^{2+} influx activates calmodulin (CaM) and downstream kinases, which impacts cytoskeleton organization and cell motility by regulating actin dynamics through the Ras–Erk pathway (Li et al., 2004; Lundberg et al., 1998). Despite the central roles played by MAPK signaling in immune responses (Stupack et al., 2000), the impact of Ras–Erk signaling on the diverse functions of immune cells has only started to be understood (Ebert et al., 2016; Scheele et al., 2007). Furthermore, in primary dendritic cells (DCs), Ras–Erk signaling remains largely unexplored (Riegel et al., 2019).

Owing to host–pathogen co-evolution by reciprocal selection, the study of host–pathogen interactions has emerged as a powerful approach to gain insight into basic cell biology. The protozoan *Toxoplasma gondii* is a model obligate intracellular pathogen due to its wide host range among warm-blooded vertebrates and its ability to actively invade nucleated cells (Sibley, 2004).

One-third of the global human population is estimated to be chronically infected with *T. gondii* (Pappas et al., 2009). Upon ingestion and after crossing the intestinal epithelium, *T. gondii* tachyzoites rapidly disseminate, ultimately establishing chronic infection in the brain (Montoya and Liesenfeld, 2004). Early on, tachyzoites encounter DCs, which play a determinant role in mounting a robust protective immune response (Liu et al., 2006). Paradoxically, *T. gondii* exploits the inherent migratory ability of DCs for dissemination via a 'Trojan horse' mechanism (Courret et al., 2006; Lambert et al., 2006, 2009; Sangare et al., 2019). Within minutes of active invasion by *T. gondii*, DCs in mice adopt a hypermigratory phenotype that mediates rapid systemic dissemination (Kanatani et al., 2017; Weidner and Barragan, 2014). We recently reported that *T. gondii* induces mesenchymal-to-amoeboid transition (MAT) in DCs (Ólafsson et al., 2018). Hypermigratory parasitized DCs are characterized by high-velocity amoeboid locomotion (termed hypermotility), cytoskeletal reorganization with loss of podosomes, decreased pericellular proteolysis and redistribution of integrins (Kanatani et al., 2015; Ólafsson et al., 2018; Weidner et al., 2013). Hypermigration is triggered by non-canonical $GABA_A$-receptor-mediated (Fuks et al., 2012) activation of VGCCs, including subtype $Ca_V1.3$ (Kanatani et al., 2017), and Timp-1-mediated, Itgb1-dependent activation of focal adhesion kinase (Fak, also known as PTK2) (Ólafsson et al., 2019). However, the signaling elements downstream of VGCC and Itgb1–Fak signaling, and their respective contribution to the hypermigratory phenotype of DCs, remain unknown.

[1]Department of Molecular Biosciences, The Wenner-Gren Institute, Stockholm University, 106 91 Stockholm, Sweden. [2]Cancer Cell Biology Laboratory, Center for Cell Biology and Biomedicine (CEBICEM), Faculty of Medicine and Science, Universidad San Sebastian, 7620001 Santiago, Chile.

*Author for correspondence (antonio.barragan@su.se)

M.V-G., 0000-0001-5857-4793; A.B., 0000-0001-7746-9964

Received 14 November 2019; Accepted 26 February 2020

Journal of Cell Science (2021) 134, jcs241752. doi:10.1242/jcs.241752

Here, we use primary DCs and *T. gondii* to investigate alternative pathways for migratory activation of immune cells. We identify Ras-dependent sustained Erk phosphorylation downstream of VGCC–CaM–CaMkII signaling and Met signaling, with an impact on non-canonical migratory activation of *T. gondii*-infected DCs. The findings provide novel mechanistic insights into infection-related MAT of DCs.

RESULTS

Erk is rapidly phosphorylated in parasitized DCs, and gene silencing of *Erk1* and *Erk2* abolishes DC hypermotility

Because the MAPKs Erk1 and Erk2 (Erk) play a key role in cancer cell metastasis (Viala and Pouyssegur, 2004) and leukocyte motility (Stupack et al., 2000), we investigated Erk activity in primary murine DCs challenged with *T. gondii* tachyzoites. We found that infection affected *Mapk3* (*Erk1*) and *Mapk1* (*Erk2*) mRNA expression (Fig. S1A). However, the total Erk protein expression of DCs was non-significantly altered upon *T. gondii* challenge 6 h post-infection (h.p.i.) (Fig. S1B). In sharp contrast, elevated Erk phosphorylation was observed at this time point, which was abrogated upon treatment with the Mek inhibitor U0126 (Fig. 1A). Because DC hypermigration begins within minutes of *T. gondii* invasion (Weidner et al., 2013), we assessed the early kinetics of Erk phosphorylation upon *T. gondii* challenge. As we found that the ratio of phosphorylated Erk to total Erk was rapidly elevated in *T. gondii*-challenged DCs (Fig. 1B), we investigated its putative role in DC hypermotility. Importantly, inhibition of Erk phosphorylation through Mek antagonism significantly decreased the mean velocity of *T. gondii*-infected DCs, without significantly impacting the baseline motility of DCs (Fig. 1C; Fig. S1C). At the concentrations used, Mek antagonism did not significantly affect DC viability, infection frequency or tachyzoite replication (Fig. S1D–G).

To determine the respective roles of Erk1 and Erk2 in DC hypermotility, we transduced DCs with lentivirus encoding an eGFP reporter and shRNA targeting *Erk1* (shErk1), *Erk2* (shErk2) or non-expressed (shLuc) mRNAs. First, the knockdown efficiency of shErk1 and shErk2 was quantified. shErk1- and shErk2-transduced DCs exhibited significantly reduced levels of *Erk1* and *Erk2* mRNA (Fig. 1D) and protein (Fig. 1E), respectively, relative to mock- and shLuc-transduced DCs. Next, the motility of transduced parasitized DCs was analyzed (Fig. 1F,G). Importantly, gene silencing of either *Erk1* or *Erk2* significantly reduced hypermotility in *T. gondii*-infected DCs and had a non-significant effect on baseline motility (Fig. 1H). From these data, we conclude that challenge of DCs with *T. gondii* is accompanied by a rapid phosphorylation of Erk that underlies *T. gondii*-mediated migratory activation of DCs.

Erk phosphorylation via Ras downstream of VGCC–CaM–CaMkII-mediated Ca^{2+} signaling governs DC hypermotility

Based on findings in neuronal cells showing that Erk is activated downstream of VGCC signaling (Kotturi et al., 2003), and because VGCCs are implicated in *T. gondii*-mediated hypermotility (Kanatani et al., 2017), we hypothesized that VGCC–Ras–Raf–Mek signaling mediated Erk phosphorylation in *T. gondii*-infected DCs. To this end, we analyzed the phosphorylation of Erk in *T. gondii*-infected DCs upon treatment with the VGCC inhibitors nifedipine (targeting L-type VGCCs) and CPCPT (a selective inhibitor of VGCC subtype $Ca_V1.3$). Interestingly, a significant inhibition of Erk phosphorylation was observed upon VGCC antagonism with both nifedipine and CPCPT in *T. gondii*-infected DCs (Fig. 2A). VGCC inhibition had a non-significant impact on the baseline phosphorylation of Erk in unchallenged DCs (Fig. S2A). Because motility-related Ras signaling is strongly associated with localized farnesylated-Ras activity at the plasma membrane (Charest et al., 2010; Sasaki et al., 2004), we pharmacologically blocked plasma membrane Ras activity. For this, we used the Ras farnesylation inhibitor salirasib and found that it significantly inhibited Erk phosphorylation in *T. gondii*-infected DCs (Fig. 2B), with a non-significant effect on baseline Erk phosphorylation (Fig. S2B). At the concentrations used, non-significant effects were observed on DC viability, infection frequencies and tachyzoite replication (Fig. S2C–E). Conversely, VGCC agonism with Bay K8644 (Bay K), a structural analog of nifedipine with a positive ionotropic effect, led to elevated Erk phosphorylation, which was inhibited by salirasib treatment (Fig. 2C). Importantly, hypermotility was abrogated by Ras antagonism (Fig. 2D,E), in line with abrogation by VGCC inhibition, $Ca_V1.3$ gene silencing (Kanatani et al., 2017) and Mek inhibition (Fig. 1C; Fig. S1C), which together indicate the involvement of a VGCC–Ras–Mek signaling axis.

Next, because calmodulin (CaM) and calmodulin kinase II (CaMkII) act downstream of VGCC-mediated Ca^{2+} influx and impact Ras–Raf activity and Erk phosphorylation (Agell et al., 2002), we investigated the putative roles of CaM and CaMkII in *T. gondii*-mediated Erk phosphorylation and DC motility. Clearly, antagonism of CaM (using w7) or CaMkII (using sto-609) significantly reduced *T. gondii*-induced Erk phosphorylation (Fig. 2F). However, a significant reduction in Erk phosphorylation was also observed in unchallenged DCs upon CaM inhibition, but not CaMkII inhibition (Fig. S2B), indicating a role for CaM in baseline Erk phosphorylation. Non-significant effects were observed on DC viability, infection frequency and tachyzoite replication (Fig. S2C–E). Importantly, CaM and CaMkII antagonism inhibited hypermotility of *Toxoplasma*-infected DCs (Fig. 2G,H). In contrast, a non-significant effect on baseline motility was noted in unchallenged DCs upon CaM inhibition and CaMkII inhibition (Fig. 2G,H). Jointly, this indicates a higher relative dependency of hypermotility on CaM–CaMkII signaling compared with baseline motility, and is consistent with the higher relative dependency of hypermotility on Erk signaling compared with baseline motility (Fig. 1C,H).

Taken together, these data indicate that L-type VGCC-$Ca_V1.3$ signal transduction occurs via the CaM–CaMkII–Ras pathway in parasitized DCs, with subsequent phosphorylation of Erk and an impact on DC migration.

Hgf–Met signaling promotes DC motility via Ras activation and Erk phosphorylation

We recently reported the involvement of the non-receptor tyrosine kinase Fak in DC hypermotility (Ólafsson et al., 2019). However, receptor tyrosine kinases (RTKs) also play central roles in cell migration and metastasis (Lemmon and Schlessinger, 2010). Because aberrantly activated RTK Met mediates metastasis in a number of cancers (Benvenuti and Comoglio, 2007; Webb et al., 1998), we investigated the expression of Met and its ligand Hgf in DCs challenged with *T. gondii*. Kinetics analyses showed that DCs upregulated the transcription of *Met* and *Hgf* mRNAs shortly after *T. gondii* challenge (Fig. S3A,B), motivating further functional investigation.

First, we investigated the impact of Met activation with recombinant Hgf (rHgf) on Erk phosphorylation and DC motility. Indeed, treatment with rHgf induced Erk phosphorylation in unchallenged DCs (Fig. 3A). Further, rHgf treatment stimulated

Journal of Cell Science (2021) 134, jcs241752. doi:10.1242/jcs.241752

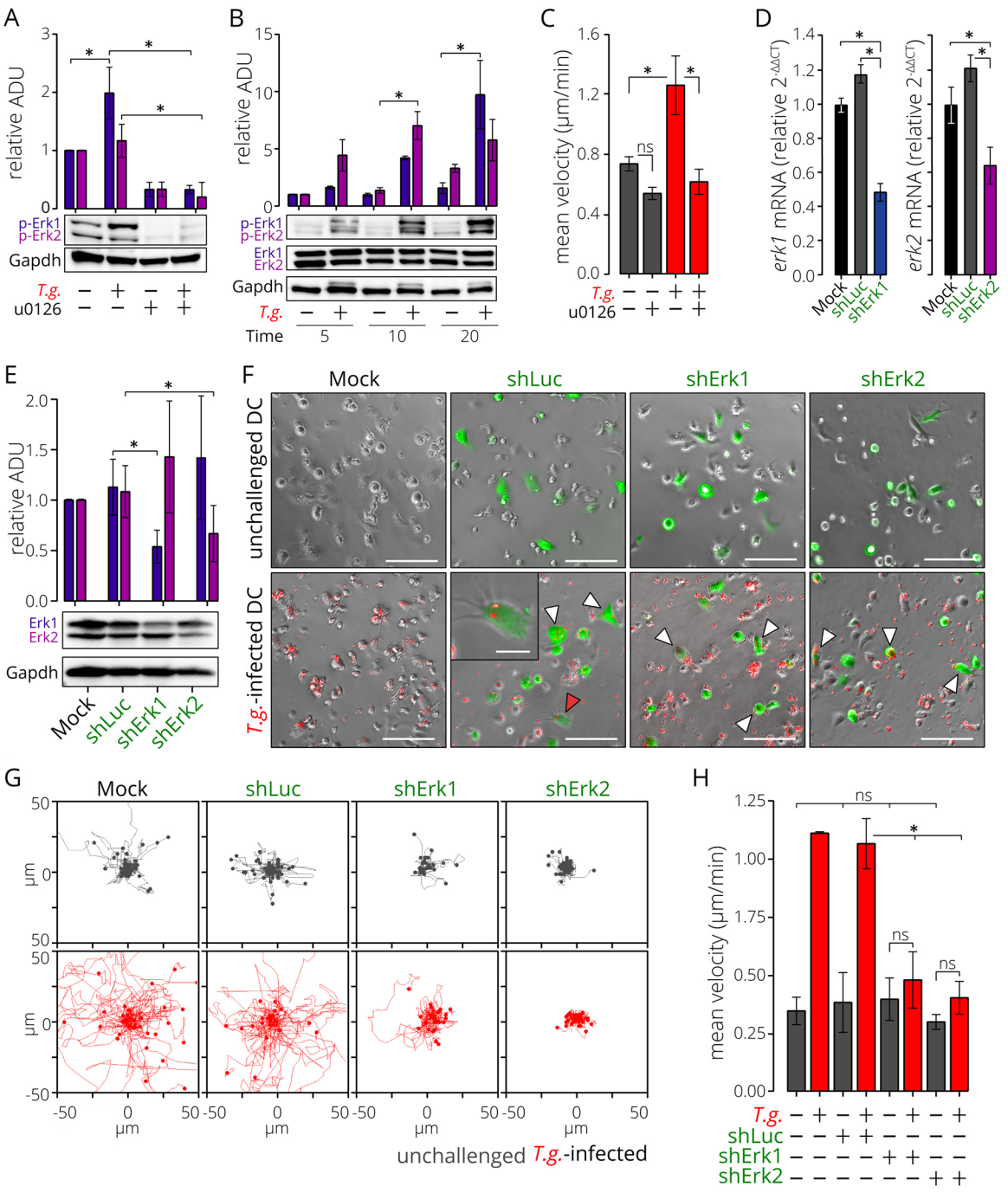

Fig. 1. See next page for legend.

motility in both unchallenged and *T. gondii*-challenged DCs (Fig. 3B). Importantly, *T. gondii*-induced Erk phosphorylation was significantly inhibited upon treatment with the Met inhibitor su11274 (targeting submembrane Met phosphorylation) and was not rescued by rHgf treatment (Fig. 3C). Moreover, inhibition of Met phosphorylation inhibited infected DC hypermotility and non-significantly affected baseline motility (Fig. 3D,E; Fig. S3C), DC viability, infection frequency and tachyzoite replication (Fig. S3E–G). Unexpectedly, challenge with *T. gondii* non-significantly affected the amounts of secreted Hgf in supernatants, relative to unchallenged DCs (Fig. 3F). Because Ras acts downstream of Met in its activation of Erk (Wang et al., 2002), and Ras antagonism inhibited hypermotility (Fig. 2E) and Erk phosphorylation (Fig. 2B), we investigated the impact of salirasib treatment on rHgf-mediated Erk phosphorylation. Similar to its inhibitory effect on VGCC-mediated Erk phosphorylation, salirasib treatment significantly inhibited rHgf-mediated Erk phosphorylation (Fig. 3G). Further, rHgf-mediated DC motility, but not baseline motility, was abolished upon treatment with salirasib, and rHgf treatment did not rescue hypermotility in salirasib-treated infected DCs (Fig. 3H). This indicates that Hgf–Met signaling impacts hypermotility via Ras.

As we did not observe elevated Hgf secretion upon *T. gondii* challenge and because *T. gondii* activates integrin Itgb1–Fak

Journal of Cell Science

Journal of Cell Science (2021) 134, jcs241752. doi:10.1242/jcs.241752

Fig. 1. Rapid phosphorylation of Erk upon *T. gondii* infection and its impact on DC hypermotility. (A) Erk phosphorylation in unchallenged and *T. gondii*-challenged DCs (*T.g.*) with or without U0126 (Mek inhibitor) treatment (10 µM) at 6 h post-infection (h.p.i.). Bar graph shows mean±s.e.m. total protein relative to Gapdh (relative arbitrary density units, ADU). Expression of unchallenged DCs was set to 1. Images show representatives of blots used for quantification, taken from the same experiment (n=8 biological replicates). (B) Erk phosphorylation in unchallenged and *T. gondii*-challenged DCs (*T.g.*) at indicated time points (minutes). Bar graph shows mean±s.e.m. phosphorylated protein relative to Gapdh (relative ADU). Expression of unchallenged DCs was set to 1. Images show representatives of blots used for quantification of total and phosphorylated Erk and Gapdh (n=4 biological replicates). (C) Bar graph shows mean±s.e.m. velocity of unchallenged and *T. gondii*-infected DCs (*T.g.*) embedded in collagen with or without U0126 treatment (10 µM; n=3 independent experiments). (D) Relative *Erk1* and *Erk2* mRNA expression (relative $2^{-\Delta Ct}$) of mock-treated, control shLuc-, shErk1- and shErk2-transduced DCs. Expression of mock-treated DCs was set to 1 (n=3 independent experiments). (E) Relative Erk1 and Erk2 total protein expression of DCs transduced with control shLuc, shErk1 or shErk2 lentivirus. Bar graph shows mean±s.e.m. Erk1 and Erk2 protein expression relative to Gapdh (relative ADU). Expression of mock-treated DCs was set to 1. Images show representatives of blots used for quantification (n=3 biological replicates). (F) Representative micrographs of mock-treated DCs (Mock) and eGFP-expressing DCs transduced with lentiviral vectors targeting *Erk1* and *Erk2* mRNA (shErk1 and shErk2, respectively) or a non-expressed target (shLuc) embedded in collagen with or without RFP-expressing *T. gondii* tachyzoites (*T.g.*). Arrowheads indicate *T. gondii*-infected cells expressing eGFP assessed in the assay, red arrowhead indicates cell shown in inset image. Scale bars: 200 µm. Inset image shows representative transduced DC (green) infected by *T. gondii* (red). Scale bar: 50 µm. Micrographs are representative of three independent experiments. (G) Representative motility plots of unchallenged and *T. gondii*-infected (*T.g.*) mock-treated, shLuc-, shErk1- and shErk2-transduced DCs embedded in collagen. Plots are representative of three independent experiments. (H) Mean±s.e.m. velocity of unchallenged and *T. gondii*-infected (*T.g.*) mock-treated, shLuc-, shErk1- and shErk2-transduced DCs embedded in collagen (n=3 independent experiments). (A–E, H) *P<0.05; n.s., not significant [one-way ANOVA, Holm–Sidak's multiple comparisons test (A,C,D,H); two-way ANOVA, Holm–Sidak's multiple comparisons test (B); paired t-test (E)].

signaling in DCs (Ólafsson et al., 2019), we hypothesized that, in addition to Hgf, Hgf-independent activation of Met might occur via Fak (Hui et al., 2009). Indeed, Erk phosphorylation was significantly reduced in *T. gondii*-infected DCs upon treatment with inhibitors targeting Fak and the associated kinase Pyk2 (Fig. 3I). The treatments had a non-significant effect on Erk phosphorylation in unchallenged DCs (Fig. S3D), DC viability, infection frequency and tachyzoite replication (Fig. S3E–G).

Taken together, the data show that Met–Ras signaling is activated in DCs upon *T. gondii* infection, with an impact on motility via phosphorylation of Erk. Further, our data suggest that, in parasitized DCs, Met is activated both by its ligand Hgf and via tyrosine kinase-mediated transactivation.

Gene silencing of *Met* inhibits hypermotility of *T. gondii*-infected DCs

To determine the role of Met in *T. gondii*-induced hypermigration, we applied a gene silencing approach in primary DCs. First, we analyzed Met protein expression in DCs by flow cytometry (Fig. S4A,B). Consistent with *Met* transcription data, signal corresponding to Met protein was significantly elevated in $CD11c^+$ DCs infected by *T. gondii* (Fig. 4A). Of note, parasitized DCs exhibited significantly higher signal corresponding to plasma membrane-associated Met and total Met compared with the signal exhibited by non-infected bystander DCs (Fig. 4A). This indicated a selective upregulation of Met in parasite-invaded DCs. Next, we silenced *Met* mRNA expression with a lentivirus encoding an eGFP reporter and shRNA targeting *Met* mRNA (shMet) or non-target control mRNA (shLuc). We confirmed that DCs transduced with shMet exhibited significantly reduced *Met* mRNA (Fig. 4B, Fig. S4C) and Met total protein (Fig. 4C) relative to shLuc transduced DCs. We then subjected Met-silenced *T. gondii*-challenged DCs to motility analyses (Fig. S4D). Importantly, gene silencing of *Met* abolished hypermotility in *T. gondii*-infected DCs (Fig. 4D,E), consistent with the effect of pharmacological antagonism of Met (Fig. 3E). Taken together, these data show that Met signaling is activated in *T. gondii*-infected DCs with an impact on motility.

DISCUSSION

In this study we investigated the putative role of the MAPKs Erk1 and Erk2 (Erk) in *T. gondii*-induced hypermigration of primary DCs. We report that *T. gondii*-induced VGCC and Met signaling converge on the Ras–Erk signaling axis to mediate hypermotility of parasitized DCs.

Our studies establish that Erk signaling plays a central role in *Toxoplasma*-induced hypermigration of DCs. A rapid and sustained Erk phosphorylation was observed upon *T. gondii* challenge, leading to the activation of DC motility. Despite transcriptional changes following infection, total Erk protein amounts remained stable, likely due to the 50 h half-life time of Erk (Schwanhausser et al., 2011). Using shRNA-mediated gene silencing of *Mapk3* and *Mapk1* and pharmacological antagonism of Erk phosphorylation (by Mek inhibition), we demonstrate that phosphorylated Erk is necessary for DC hypermotility. Interestingly, knockdown of either Erk1 or Erk2 was sufficient for reducing hypermotility (although baseline motility was maintained), despite shared substrate redundancy between Erk1 and Erk2 (von Kriegsheim et al., 2009). This indicates a dependency on both Erk isoforms for hypermotility but not for baseline DC motility. Moreover, the observed compensatory elevation of Erk1 expression upon silencing of *Erk2*, and elevation of Erk2 upon silencing of *Erk1*, were not sufficient to maintain hypermotility. This rapid reciprocal compensatory expression between Erk1 and Erk2 advocates for a tight regulation of the Erk MAPK pathway in primary DCs. Furthermore, the crucial dependence of DC hypermotility on Erk signaling cannot be generalized to other MAPK pathways as, for example, infected DCs remain hypermotile upon inhibition of the MAPK p38 (ten Hoeve et al., 2019). Taken together, these observations prompted us to investigate signaling pathways upstream of Erk activation in parasitized DCs.

Our data show that VGCC–CaM–CaMkII–Ras signaling acts upstream of Erk to mediate migratory activation of DCs. Previously, we showed that the onset of the hypermigratory phenotype in DCs depends on live intracellular parasites and the discharge of *T. gondii* secretory organelles, independently of TLR–MyD88 signaling or chemotaxis (Fuks et al., 2012; Lambert et al., 2006; Ólafsson et al., 2018; Sangare et al., 2019; Weidner et al., 2013). However, TLR–MyD88 signaling and chemotactic stimuli can also activate Erk. Specifically, in *T. gondii*-infected macrophages both TLR–MyD88-dependent and a strong component of TLR–MyD88-independent Erk activation have been described (Kim et al., 2006). However, *T. gondii*-induced hypermigration is fully maintained in MyD88-deficient DCs (Lambert et al., 2006; Ólafsson et al., 2018). Similarly, hypermigration is independent of chemotactic stimuli (but can act synergistically with chemotaxis upon stimulation) (Fuks et al., 2012; Kanatani et al., 2015; Weidner et al., 2013). Thus, alternative signaling underlies the migratory activation of DCs by *T. gondii* and, consequently, the hypermotility-related activation of Erk observed here.

Journal of Cell Science (2021) 134, jcs241752. doi:10.1242/jcs.241752

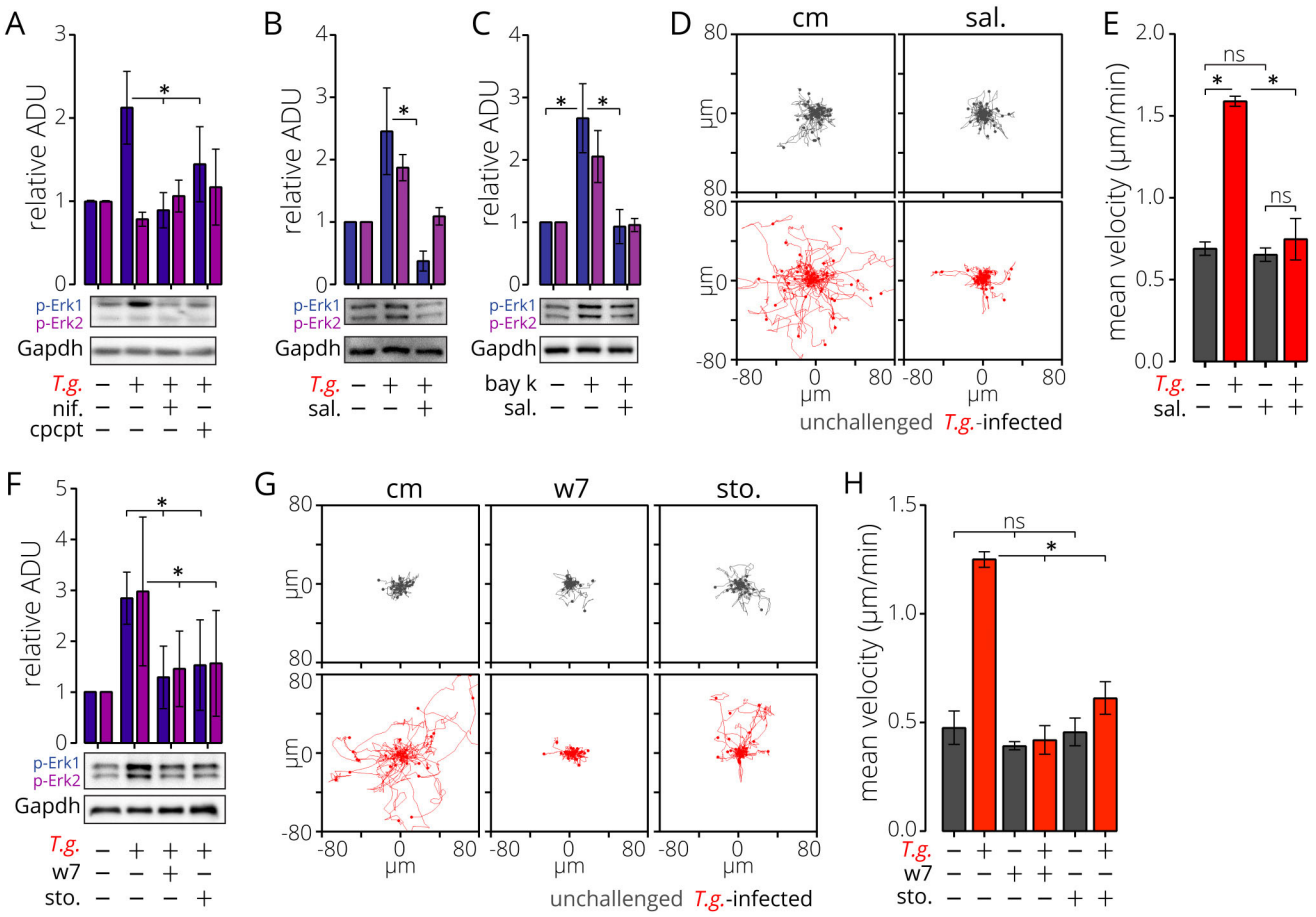

Fig. 2. Activation of VGCCs mediates Erk phosphorylation through CaM–CaMkII–Ras and impacts DC motility. (A) Erk phosphorylation in unchallenged and *T. gondii*-challenged DCs (*T.g.*) with or without nifedipine (nif., L-VGCC inhibitor, 50 µM) or CPCPT ($Ca_V1.3$ inhibitor, 10 µM) treatment at 2 h.p.i. Bar graph shows mean±s.e.m. phosphorylated Erk1 and Erk2 protein relative to Gapdh (relative arbitrary density units, ADU). Expression of unchallenged DCs was set to 1. Images show representatives of blots used for quantification, taken from the same experiment (n=3 biological replicates). (B) Erk phosphorylation in unchallenged and *T. gondii*-challenged DCs (*T.g.*) with or without salirasib (sal., Ras farnesyltransferase inhibitor, 100 µM) at 2 h.p.i. Bar graph shows mean±s.e.m. phosphorylated Erk1 and Erk2 protein relative to Gapdh (relative ADU). Expression of unchallenged DCs was set to 1. Images show representative blots taken from the same experiment and used for quantification (n=3 biological replicates). (C) Erk phosphorylation in unchallenged DCs with or without Bay K (L-VGCC agonist, 10 µM) and salirasib (sal., 100 µM) 20 min post-treatment. Bar graph shows mean±s.e.m. phosphorylated Erk1 and Erk2 protein relative to Gapdh (relative ADU). Expression of unchallenged DCs was set to 1. Representative blots are shown (n=4 biological replicates). (D) Representative motility plots of unchallenged and *T. gondii*-infected DCs (*T.g.*) embedded in collagen in CM (complete medium) with or without salirasib (sal., 25 µM). Plots are representative of three independent experiments. (E) Bar graph shows mean±s.e.m. velocity of unchallenged and *T. gondii*-infected DCs (*T.g.*) embedded in collagen treated as in D (n=3 independent experiments). (F) Erk phosphorylation in unchallenged and *T. gondii*-challenged DCs (*T.g.*) with or without w7 (CaM inhibitor, 25 µM) or sto-609 (sto., CaMkII inhibitor, 50 µM) treatment at 2 h.p.i. Bar graphs show mean±s.e.m. phosphorylated Erk1 and Erk2 protein relative to Gapdh (relative ADU). Expression of unchallenged DCs was set to 1. Images show representative blots (n=4 biological replicates). (G) Representative motility plots of unchallenged and *T. gondii*-infected DCs (*T.g.*) embedded in collagen in CM with or without w7 (25 µM) or sto-609 (sto., 25 µM). Plots are representative of three independent experiments. (H) Bar graph shows mean±s.e.m. velocity of unchallenged and *T. gondii*-infected DCs (*T.g.*) embedded in collagen treated as in G (n=3 independent experiments). (A–C, E,F,H) *P<0.05; n.s, not significant [one-way ANOVA, Tukey's HSD post-hoc test (A–C,E,H); one-way ANOVA, Holm–Sidak's multiple comparisons test (F)].

T. gondii promotes DC hypermigration via GABAergic signaling (Fuks et al., 2012), which triggers the activation of the VGCC $Ca_V1.3$ (Kanatani et al., 2017). VGCC-mediated Ca^{2+} influx impacts Ca^{2+}-sensing proteins locally at the cell membrane (Rosen et al., 1994; Zhou et al., 2015). Here, by pharmacological agonism and antagonism of the VGCC signaling axis, we extend these findings by linking Erk phosphorylation to VGCC activation and CaM–CaMkII–Ras signaling. We show that inhibition of L-type VGCCs and $Ca_V1.3$ with nifedipine and CPCPT, respectively, effectively blocked Erk phosphorylation in *T. gondii*-infected DCs. We previously showed that VGCC agonism enhances migration of unchallenged and *T. gondii*-challenged DCs (Kanatani et al., 2017). Importantly, reinforcing the link between VGCCs, and specifically $Ca_V1.3$, and Erk, we show that L-type VGCC agonism (Bay K) enhanced Erk phosphorylation via CaM–CaMkII–Ras signaling whereas the opposite effect was observed upon antagonism (nifedipine, CPCPT). These data are in line with paradigms in neuronal cells, where VGCC-dependent CaM activity regulates cytoskeleton organization and cell migration via Ras–Erk signaling (Rosen et al., 1994). Further, in lymphocytes, treatment with nifedipine and Bay K blocks and stimulates Erk phosphorylation, respectively (Kotturi et al., 2003). Thus, our data describe, for the first time, VGCC ($Ca_V1.3$)-mediated Erk activation in leukocytes and provide evidence for its dependence on CaM–CaMkII–Ras signaling.

Cancer cells seldom rely on one single pathway to orchestrate metastasis. Instead, metastasis generally relies on the activation of redundant and complementary pathways (Tracey et al., 2013).

Journal of Cell Science (2021) 134, jcs241752. doi:10.1242/jcs.241752

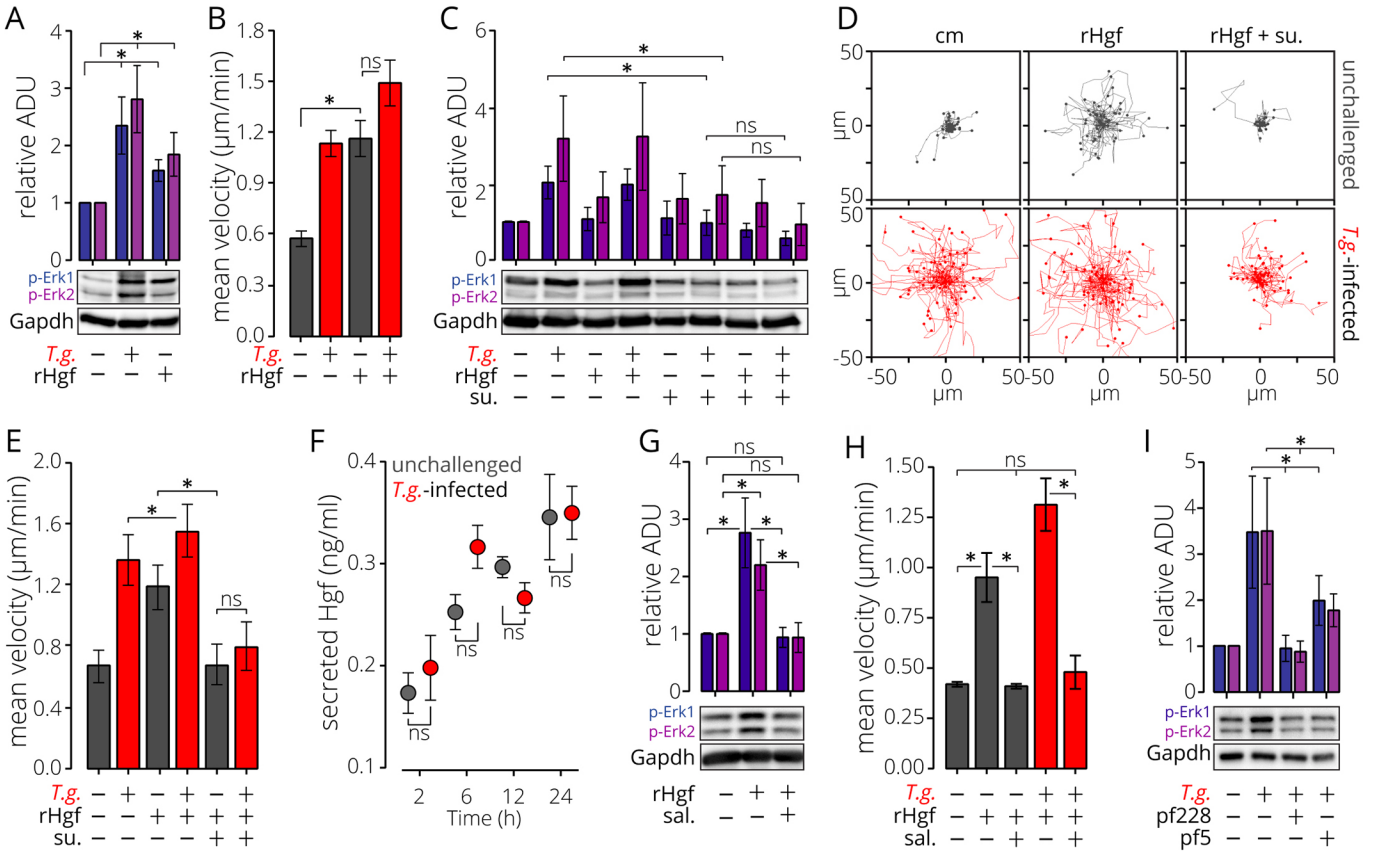

Fig. 3. Erk phosphorylation downstream of Hgf–Met via Ras signaling impacts DC hypermotility. (A) Erk phosphorylation in unchallenged and *T. gondii*-challenged DCs (*T.g.*) with or without recombinant-Hgf (rHgf, 40 ng/ml) treatment at 2 h.p.i. Bar graph shows mean±s.e.m. phosphorylated protein relative to Gapdh (relative arbitrary density units, ADU). Expression of unchallenged DCs was set to 1. Images show representatives of blots used for quantification, taken from the same experiment (n=6 biological replicates). (B) Mean velocity of unchallenged and *T. gondii*-infected DCs (*T.g.*) embedded in collagen with or without rHgf (40 ng/ml) treatment. Data are presented as mean±s.e.m. from three experiments. (C) Erk phosphorylation in unchallenged and *T. gondii*-challenged DCs (*T.g.*) with or without rHgf (40 ng/ml), su11274 (su., Met inhibitor, 10 µM) or combined rHgf and su11274 treatment at 6 h.pi. Bar graph shows mean±s.e.m. phosphorylated protein relative to Gapdh (relative ADU). Expression of unchallenged DCs was set to 1. Images show representative blots (n=4 biological replicates). (D) Representative motility plots of unchallenged and *T. gondii*-infected DCs (*T.g.*) embedded in collagen in CM with or without rHgf (40 ng/ml), su11274 (10 µM) or combined rHgf and su11274 treatment. Plots are representative of three independent experiments. (E) Bar graph shows mean±s.e.m. velocity of unchallenged and *T. gondii*-infected DCs (*T.g.*) embedded in collagen treated as in D (n=3 independent experiments). (F) Secreted Hgf protein in supernatants from unchallenged and *T. gondii*-challenged DCs (*T.g.*-infected) collected at 2, 6, 12 and 24 h.p.i. Data are presented as mean±s.e.m. from three experiments. (G) Erk phosphorylation in unchallenged DCs with or without rHgf (40 ng/ml) or rHgf and salirasib (sal., 100 µM) at 20 min post treatment. Bar graph shows mean±s.e.m. phosphorylated Erk1 and Erk2 protein relative to Gapdh (relative ADU). Expression of unchallenged DCs was set to 1. Images show representative blots (n=4 biological replicates). (H) Mean velocity of unchallenged and *T. gondii* (*T.g.*)-infected DCs embedded in collagen with or without rHgf (40 ng/ml) or rHgf (40 ng/ml) and salirasib (sal., 100 µM) treatment. Data are presented as mean±s.e.m. from three independent experiments. (I) Erk phosphorylation in unchallenged and *T. gondii*-challenged DCs (*T.g.*) with or without pf228 (Fak inhibitor, 10 µM) or pf5 (Fak and Pyk2 inhibitor, 10 µM) treatment 2 h.p.i. Bar graph shows mean±s.e.m. phosphorylated protein relative to Gapdh (relative ADU). Expression of unchallenged DCs was set to 1. Images show representative blots (n=3 biological replicates). (A–C,E–I) *P<0.05; n.s., not significant. [one-way ANOVA, Tukey's HSD post-hoc test (A,B,E,G–I); paired *t*-test (C); two-way ANOVA, Holm–Sidak's multiple comparisons test (F)].

Consequently, we reasoned that diverse signaling cascades might underlie hypermotility in parasitized DCs.

Here, we identify a role for the receptor tyrosine kinase Met in the migratory activation of primary DCs. Upon *T. gondii* challenge, transcriptional upregulation and increased Met protein expression was indicative of activation. Importantly, antagonism of Met and gene silencing of *Met* inhibited DC hypermotility. Functionally reinforcing the observation that Met is upregulated on the plasma membrane of parasitized DCs, rHgf treatment and infection had a synergistic effect on migratory activation. Furthermore, treatment with rHgf induced Erk phosphorylation and motility in unchallenged DCs. Conversely, Met antagonism inhibited Erk phosphorylation in unchallenged rHgf-treated DCs and *T. gondii*-infected DCs. Finally, Ras inhibition blocked rHgf–Met-induced Erk phosphorylation. Consistent with this idea, aberrant Met signaling mediates invasive cell growth and metastasis (Benvenuti and Comoglio, 2007) and afferent lymphatic migration of epidermal DCs upon skin inflammation (Baek et al., 2012). Altogether, our data demonstrate that Met mediates migratory activation of DCs through Ras–Erk signaling.

Because Hgf is the only known ligand for Met, we investigated the secretion of Hgf by DCs upon *T. gondii* challenge. Surprisingly, the concentration of Hgf in supernatant from DCs was non-significantly affected by *T. gondii* challenge, suggesting that alternative mechanisms activate Met signaling in *T. gondii*-infected DCs. Ligand-independent activation of Met, or transactivation, is regulated by adapter proteins, integrins and tyrosine kinase crosstalk (Fischer et al., 2004; Hui et al., 2009; Mitra et al., 2011). Pharmacological antagonism of Fak and Pyk2 blocked Erk phosphorylation to a similar extent to Met antagonism in *T. gondii*-infected DCs, providing evidence for tyrosine kinase-

Journal of Cell Science (2021) 134, jcs241752. doi:10.1242/jcs.241752

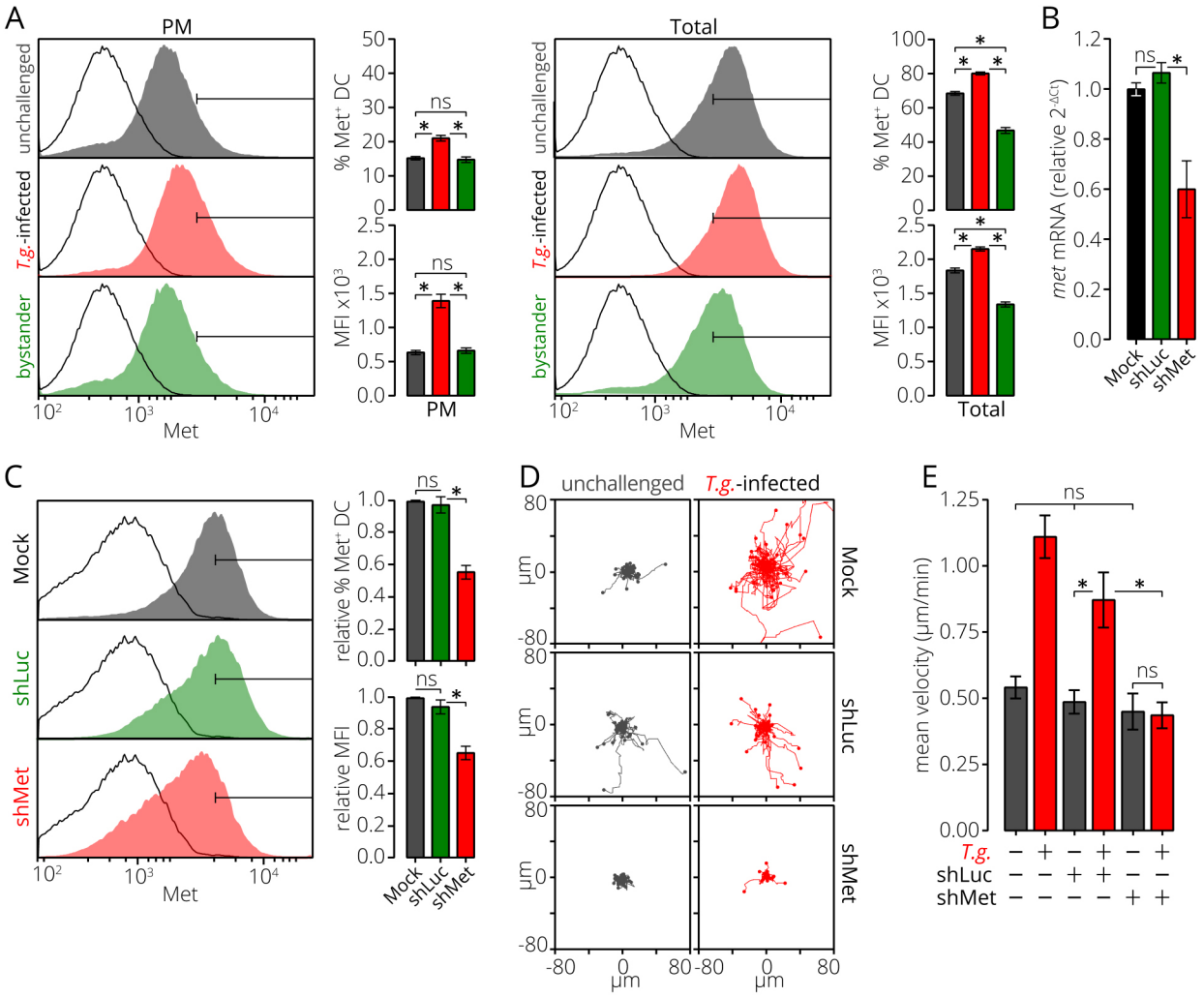

Fig. 4. Expression of Met is upregulated in parasitized DCs and gene silencing of *Met* inhibits hypermotility. (A) Plasma membrane (PM, left histograms) and total (right histograms) Met protein expression of CD11c$^+$ unchallenged (gray), *T. gondii*-infected (*T.g.*, red) and non-infected bystander (green) DCs. Histograms show gate used to define Met$^+$ cells. Black line represents isotype control for Met. Bar graphs show mean±s.e.m. percentage of Met$^+$ cells and Met median fluorescence intensity (MFI) for each population (n=4 independent experiments). (B) Mean±s.e.m. relative *Met* mRNA expression ($2^{-\Delta Ct}$) of mock-treated, control shLuc- and shMet-transduced DCs. Expression of mock-treated DCs was set to 1 (n=3 independent experiments). (C) Met protein expression of CD11c$^+$ mock-treated DCs and DCs transduced with control shLuc or shMet lentivirus. Gating performed as in A. Histogram shows gate used to define Met$^+$ cells. Gray, green and red fill show mock-treated, shLuc-transduced and shMet-transduced DCs, respectively. Black line represents isotype control. Bar graphs show mean±s.e.m. percentage of Met$^+$ cells and Met MFI for each population (n=3 independent experiments). (D) Representative motility plots of unchallenged and *T. gondii*-infected (*T.g.*) mock-treated, shLuc-, shMet-transduced DCs embedded in collagen. Plots are representative of three independent experiments. (E) Mean±s.e.m. velocity of unchallenged and *T. gondii*-infected (*T.g.*) mock-treated, shLuc- or shMet-transduced DCs embedded in collagen (n=6–8 independent experiments). (A–C,E) *P<0.05; n.s., not significant (one-way ANOVA, Tukey's HSD post-hoc test).

mediated transactivation of Met. In breast cancer cells, the integrin Itgb1 transactivates Met (Barrow-McGee et al., 2016). We recently described a Timp-1–CD63–Itgb1–Fak signaling axis in *T. gondii*-infected DCs, and found gene silencing and antagonism of Itgb1 and Fak abolished hypermotility (Ólafsson et al., 2019). Furthermore, Timp-1 was recently shown to promote activation of the RTK c-Kit in DLD-1 colorectal cancer cells (Nordgaard et al., 2019). Taken together, the data advocate for a potentiation of the motogenic action of Met through the Timp-1–CD63–Itgb1–Fak axis. However, additional possibilities that are not mutually exclusive with this idea exist. The secreted *T. gondii* proteins MIC1, MIC3 and MIC6 can directly phosphorylate the RTK Egfr (Muniz-Feliciano et al., 2013), which could hypothetically contribute to Met transactivation. Collectively, the data demonstrate that *T. gondii* activates the Met signaling pathway in infected DCs. Consistent with results from our previous studies, a milieu of RTK crosstalk with Erk phosphorylation in *T. gondii*-infected immune cells emerges, reminiscent of that described in metastatic cancer cells (Kaufmann et al., 2009; Volinsky and Kholodenko, 2013).

The data raise questions on how the regulation of hypermigration is fine tuned. Amoeboid hypermigration of parasitized DCs represents a dramatic activation of DC locomotion, which is sustained over time and integrates multiple cell signaling pathways (Fuks et al., 2012; Kanatani et al., 2015; Ólafsson et al., 2018; Weidner et al., 2013). Notably, blockade of VGCC–Ras signaling or Met–Ras signaling independently leads to inhibition of hypermotility, but not baseline motility of DCs. We speculate that the onset and maintenance of hypermigration requires a threshold signaling activity that is achieved by co-engaging tightly regulated VGCC and Met RTK signaling. Supporting this concept, in neuronal models, VGCC and NGF RTK signaling synergistically converge on Ras for neuronal survival (Vaillant et al., 1999).

Journal of Cell Science (2021) 134, jcs241752. doi:10.1242/jcs.241752

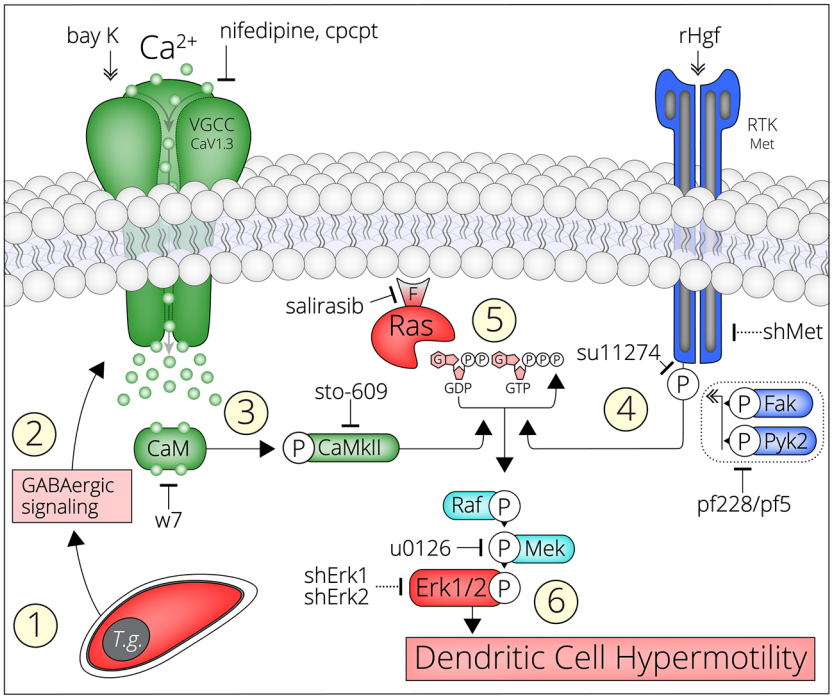

Fig. 5. Model for Erk-mediated migratory activation of *T. gondii*-infected DCs via VGCC–Ras and Met–Ras signaling. (1) *T. gondii* (*T.g.*) actively invades DCs and resides in a parasitophorous vacuole. (2) Within 5 min of parasite invasion (Weidner et al., 2013), hypermotility is triggered in DCs through GABAergic signaling (Fuks et al., 2012). (3) GABAergic signaling triggers membrane depolarization, which activates VGCCs (chiefly $Ca_V1.3$) and leads to Ca^{2+} influx. Gene silencing of $Ca_V1.3$ (but not $Ca_V1.2$) abrogates hypermotility (Kanatani et al., 2017). Inhibition of L-type VGCCs or $Ca_V1.3$ with nifedipine and CPCPT, respectively, abolishes *T. gondii*-induced Erk phosphorylation and hypermotility. Similarly, inhibition of the VGCC signal transduction proteins CaM (w7) and CaMkII (sto-609) inhibits Erk phosphorylation and hypermotility. 'P' indicates protein phosphorylation. (4) RTK Met expression in DCs is upregulated upon *T. gondii* infection and secretion of its ligand Hgf is maintained. Inhibition of Met phosphorylation (su11274) blocks Erk phosphorylation in *T. gondii*-infected DCs. Activation of Met with recombinant Hgf (rHgf) induces hypermotility and Erk phosphorylation in unchallenged and *T. gondii*-challenged DCs. Inhibition of Met phosphorylation (su11274) and gene silencing of *Met* (shMet) abolish hypermotility. The integrin Itgb1 activates Fak upon *T. gondii* infection of DCs and gene silencing of *Itgb1* and *Fak* (*Ptk2*) inhibit hypermotility (Ólafsson et al., 2019). Inhibition of the tyrosine kinases Fak and Pyk2 (pf228, pf5) blocks Erk phosphorylation, supporting tyrosine kinase-mediated transactivation of Met. (5) VGCC-mediated Ca^{2+} influx and Met signaling converge on Ras GTPase. Antagonism of Ras farnesylation (indicated by 'F') with salirasib, inhibits Ras localization to the plasma membrane and its transition to activated form (GDP to GTP). Ras antagonism blocks agonist-induced (Bay K) VGCC-mediated Erk phosphorylation and hypermotility. Similarly, Ras antagonism blocks rHgf-induced Met-mediated Erk phosphorylation and hypermotility. (6) Erk1/2 is rapidly phosphorylated in *T. gondii*-infected DCs downstream of Ras via Raf and Mek MAPKs. Antagonism of Mek (U0126) inhibits Erk phosphorylation and hypermotility in parasitized DCs. Furthermore, gene silencing of *Erk1* (shErk1) and *Erk2* (shErk2) abolishes hypermotility. Hypothetically, activated Erk regulates targets in the cytosol and also translocates to the nucleus to regulate gene expression, to maintain the DC in a hypermotile state.

Additionally, cross-regulation between VGCC and RTK signaling may take place (Cullen and Lockyer, 2002; Vela et al., 2007).

For the experimental conditions used, the pharmacological inhibitors had a non-significant effect on DC viability and parasite replication. However, an impact on the secretion of putative parasite-derived effectors by pharmacological inhibitors, or subtle effects on parasite metabolism without an impact on viability, cannot be ruled out. However, the inhibitor data is consistent with gene silencing data targeting effectors of the host cell. The data are also in line with previous work targeting upstream components of the two converging signaling pathways by gene silencing and with pharmacological modulators (Fuks et al., 2012; Kanatani et al., 2017; Ólafsson et al., 2019).

Based on our data, we propose a model for the migratory activation of DCs upon challenge with *T. gondii* (Fig. 5). *T. gondii* infection activates Ras signaling through Met and $GABA_AR$–VGCC–CaM–CaMkII signaling. Subsequently, the Ras–Raf–Mek cascade phosphorylates Erk, which drives migratory activation in DCs. The data show that *T. gondii* orchestrates the migratory activation of parasitized DCs through the Ras–Erk signaling node, which in turn is activated via tyrosine kinase signaling, integrins and GABA/Ca^{2+} ion channel activation (Kanatani et al., 2017; Ólafsson et al., 2019). Our data also provide a molecular basis for the MAT and hypermigration of parasitized DCs. Interestingly, amoeboid motility is a feature of metastasizing cells, and the signaling in parasitized DCs is consistent with emerging paradigms of signaling in metastatic cells (Lambert et al., 2017). Future studies will unravel the downstream effectors of Erk1 and Erk2 in DC hypermotility. In this context, putative parasite-derived effectors have recently been identified, which may interact with host cell MAPK signaling (Weidner et al., 2016), WAVE complex and actin dynamics (Sangare et al., 2019), and Rho GTPases (Drewry et al., 2019) in infected leukocytes. Thus, our data provide a signaling framework for assessing parasite-derived effectors and non-canonical migratory activation of leukocytes. Future investigations need to address how putative effectors emanating from rhoptries and dense-granule organelles impact the onset and regulation of the hypermigratory phenotype of parasitized phagocytes. Finally, this work highlights conserved signaling mechanisms between neurons, metastasizing cells and immune cells in the context of infection, which should be taken into consideration when designing therapies that target Met, VGCCs or Ras–Erk signaling.

Journal of Cell Science (2021) 134, jcs241752. doi:10.1242/jcs.241752

MATERIALS AND METHODS

Ethics statement

The Regional Animal Research Ethical Board, Stockholm, Sweden, approved experimental procedures and protocols involving extraction of cells from mice, following proceedings described in EU legislation (Council Directive 2010/63/EU).

Cells and parasites

Murine bone marrow-derived DCs (DCs) were generated as previously described (Lambert et al., 2006). Briefly, cells from bone marrow of 6–10-week-old male or female C57BL/6 mice (Charles River) were cultivated in RPMI 1640 with 10% fetal bovine serum (FBS), gentamicin (20 µg/ml), glutamine (2 mM) and HEPES (0.01 M) – referred to as complete medium (CM; all reagents from Life Technologies) – and supplemented with recombinant mouse GM-CSF (10 ng/ml; Peprotech). Loosely adherent cells were harvested after 6–10 days of maturation. *T. gondii* tachyzoites of the RFP-expressing Prugniaud strain (Pru and Pru-RFP, type II) (Lambert et al., 2009) or GFP-expressing Ptg strain (type II) (Weidner et al., 2013) lines were maintained by serial 2-day passages in human foreskin fibroblast (HFF-1 SCRC-1041, American Type Culture Collection) monolayers. Cell and parasite cultures were periodically tested for mycoplasma (Biontex). The hypermigratory phenotype induced by type II strains in DCs has been previously characterized (Ólafsson et al., 2018).

Reagents

The following soluble reagents were used to treat DCs in motility assays and for samples analyzed by western blotting: w-7 hydrochloride (w7, 25 µM, Tocris), sto-609 acetate (sto., 25–50 µM, Tocris), rHgf (40 ng/ml, Sigma-Aldrich), su11274 (su., 10 µM, Tocris), U0126 (10 µM, Tocris), salirasib (sal., 25–100 µM, Tocris), nifedipine (nif., 50 µM, Sigma-Aldrich), 1-(3-Chlorophenethyl)- 3-cyclopentylpyrimidine-2,4,6-(1H,3H,5H)-trione (cpcpt, 10 µM, Sigma-Aldrich), bay K8644 (Bay K, 10 µM, Sigma-Aldrich), pf573228 (pf228, 10µM, Tocris), pf562271 (pf5, 10 µM, Selleckchem).

Lentiviral vector production and *in vitro* transduction

Self-complementary hairpin DNA oligonucleotides targeting mouse *Met* (shMet), *Erk1* (shErk1) *Erk2* (shErk2) mRNA, and a non-related sequence shRNA control (shLuc) were chemically synthesized (DNA Technology, Denmark), aligned and ligated in a self-inactivating lentiviral vector (pLL3.7) containing a CMV-driven eGFP reporter and a U6 promoter upstream of cloning restriction sites (HpaI and XhoI) (Table S1). Lentivirus production was performed using Lipofectamine transfection. Briefly, shLuc, shMet, shErk1 or shErk2 vectors were co-transfected with the packaging vector psPAX2 (12260, Addgene) and envelope vector pCMV-VSVg (8454, Addgene) into HEK293FT or HEK293T Lenti-X cells (Takara Bio) and the resulting supernatant was collected after 48–72 h. The supernatant was centrifuged at 3000 ***g*** for 15 min to eliminate cell debris, filtered through 0.45 mm cellulose acetate filters, and virus particles were concentrated by ultracentrifugation at 50,000 ***g*** for 1 h, then resuspended in RPMI. Titers were determined by infecting HEK293FT cells with serial dilutions of concentrated lentivirus and determination of percentage of infected cells by flow cytometry (FACS Fortessa, BD Biosciences). Bone marrow-derived DCs were transduced twice at a multiplicity of infection (MOI) of 1 on day 3 and 4, or once at MOI 2 on day 3 by spinoculation at 1200 ***g*** for 2 h. Three days post-transduction eGFP-expression was verified by epifluorescence microscopy before the cells were used in experiments.

Motility assays

Motility assays were performed as previously described (Ólafsson et al., 2019). Briefly, DCs were cultured in 96-well plates with CM±freshly egressed *T. gondii* tachyzoites (Pru-RFP for shRNA experiments and Ptg-GFP for all other experiments, MOI 3, 4 h) and soluble reagents as indicated. Bovine collagen I (1 mg/ml, Life Technologies) was then added and live cell imaging was performed for 1 h, 1 frame/min, using a 10× objective (Z1 Observer with Zen 2 Blue v. 4.0.3, Zeiss). Time-lapse images were consolidated into stacks and motility data was obtained from >30 cells/condition (Manual Tracking, ImageJ) yielding mean velocities (Chemotaxis and migration tool, v. 2.0, Ibidi). Infected DCs were defined by localization of tachyzoite-derived RFP or GFP fluorescence within the cell boundary. Transduced cells were defined by the expression of eGFP.

Quantitative PCR

DCs were cultured in CM with or without freshly egressed *T. gondii* tachyzoites (Ptg-GFP, MOI 3). Total RNA was extracted using TRIzol reagent (Invitrogen). Quantitative PCR was performed using SYBR Green PCR master mix (Kapa Biosystems), forward and reverse primers (200 nM) and cDNA (100 ng) and run on the Rotor Gene 6000 system (Corbett) for 45 cycles. Amplicons were validated with melting curves and agarose gel (1%) analysis. Data was analyzed with RG-6000 application software (v1.7, Corbett). *Gapdh* and *Actb* were used as housekeeping genes to generate ΔCt values. $2^{(-\Delta Ct)}$ values were generated to show relative knockdown efficiency and $2^{(-\Delta\Delta Ct)}$ values were used to show expression fold-change upon infection. Fold changes in expression were calculated using the comparative DCT method against the non-infected DC control. Primers were designed using Getprime (David et al., 2017) (Table S2) and purchased from Invitrogen.

Flow cytometry and viability assays

DCs were cultured in CM with or without freshly egressed *T. gondii* tachyzoites (Ptg-GFP, MOI 3, 4 h). Following Fc blockade (clone 2.4G2, Cat. #553141, BD Pharmingen), cells were stained with anti-CD11c-PE-Cy7 (clone N418, Cat. #25-0114-82, eBiosciences). After fixation (PFA 4%), cells were either directly stained (to detect plasma membrane Met) or permeabilized (IntraPrep Permeabilization kit, Cat. #IM2389, Beckman Coulter) before staining (to detect total Met). For staining we used anti-Met-PE (clone eBioclone 7, Cat. #12-8854-82, eBiosciences) or isotype control (clone eBRG1, Cat. #14-4301-82, eBiosciences). All antibodies were used at a dilution of 1:100. Samples were run on a BD LSRFortessa Cell Analyzer (BD Biosciences). Data was analyzed in FlowJo (Tree Star Inc, OR).

For infection frequencies, DCs were cultured in CM±reagents (as indicated) and freshly egressed *T. gondii* tachyzoites (Ptg-GFP, MOI 3) for 2 h. After fixation (PFA 4%), samples were run on an easyCyte™ 8HT (Millipore), in accordance with the manufacturer's guidelines. Samples were gated on FSC, SSC and GFP. A minimum of 30,000 cells were analyzed per condition. Data were analyzed in FlowJo (Tree Star Inc, OR). Fluorescence interference of su11274 precluded determination of infection frequency with this reagent. DC viability was assessed by flow cytometry (FACS Fortessa, BD) using LIVE/DEAD Fixable Violet staining (Cat. #L34963, Thermo Fisher Scientific) in the BV-421 channel. Sto-609 exhibited fluorescence in the BV-421 channel and was therefore assessed with adapted gating. Parasite replication was assessed on HFF monolayers after 24 h by counting 100 vacuoles/condition using epifluorescence microscopy (Z1 Observer with Zen 2 Blue v. 4.0.3, Zeiss) as detailed in Ólafsson et al. (2019).

Hgf ELISA

Supernatants from DCs cultured in CM with or without freshly egressed *T. gondii* tachyzoites (Ptg-GFP, MOI 3) were collected at 2, 6, 12 or 24 h post-infection. Samples were analyzed by ELISA (MHG00, Thermo Fisher Scientific) according to the manufacturer's instructions. Samples were normalized to a CM control.

Western blotting

Cell lysates were collected and sonicated in RIPA buffer (150 mM NaCl, 5 mM EDTA, pH 8.0, 50 mM Tris-HCl, pH 8.0, 0.1% Triton-X100, 0.5% sodium deoxycholate and 0.1% SDS) with protease and phosphatase inhibitors (Thermo Fisher Scientific). Proteins were separated on 10% SDS-PAGE gels followed by transfer to PVDF Immobilon membranes (Millipore). Phospho-Erk was detected using an anti-phospho-Erk antibody (1:1000, clone D13.14.4E, Cat. #4370, Cell Signaling Technology), total Erk was detected using an anti-Erk antibody (1:2000, clone 137F5, Cat. #4695, Cell Signaling Technology) and Gapdh was detected with an anti-Gapdh antibody (1:3000, Cat. #ABS16, Millipore). HRP-conjugated anti-rabbit-IgG (1:3000, Cat. #7074S, Cell Signaling Technology) was used as secondary antibody. Proteins were visualized using ECL reagents (GE healthcare) in a Biorad ChemiDoc XRS^{+}. Densitometry analysis was performed using ImageJ (NIH, MD).

Statistical analyses

Multiple comparisons of normally distributed data were carried out with one-way ANOVA followed by Tukey's HSD, Holm–Sidak's or Dunnett's multiple comparisons test. Two-way ANOVA followed by Holm–Sidak's multiple comparisons test was used to evaluate the interaction between time and infection. Two sample comparisons were carried out with paired or unpaired *t*-tests. Normality was tested by the Shapiro–Wilks test. In all statistical tests P-values<0.05 were defined as significant. All statistics were performed with Prism (v. 8, Graphpad).

Acknowledgements

We thank all members of the Barragan laboratory for critical input.

Competing interests

The authors declare no competing or financial interests.

Author contributions

Conceptualization: E.B.Ó., A.B.; Methodology: E.B.Ó., A.L.t.H., X.L.-W., L.W., M.V.-G.; Validation: M.V.-G., A.B.; Formal analysis: E.B.Ó., A.L.t.H.; Investigation: E.B.Ó., A.L.t.H., X.L.-W., L.W.; Data curation: E.B.Ó.; Writing - original draft: E.B.Ó., A.B.; Writing - review & editing: E.B.Ó., A.B.; Visualization: E.B.Ó.; Supervision: A.B.; Project administration: A.B.; Funding acquisition: A.B.

Funding

This work was funded by the Swedish Research Council (Vetenskapsrådet, 2018-02411 to A.B.) and the Olle Engkvist Foundation (Stiftelsen Olle Engkvist Byggmästare, 193-609 to A.B.).

Supplementary information

Supplementary information available online at
http://jcs.biologists.org/lookup/doi/10.1242/jcs.241752.supplemental

Peer review history

The peer review history is available online at
https://jcs.biologists.org/lookup/doi/10.1242/jcs.241752.reviewer-comments.pdf

References

Agell, N., Bachs, O., Rocamora, N. and Villalonga, P. (2002). Modulation of the Ras/Raf/MEK/ERK pathway by Ca^{2+}, and calmodulin. *Cell. Signal.* **14**, 649-654. doi:10.1016/S0898-6568(02)00007-4

Baek, J.-H., Birchmeier, C., Zenke, M. and Hieronymus, T. (2012). The HGF receptor/Met tyrosine kinase is a key regulator of dendritic cell migration in skin immunity. *J. Immunol.* **189**, 1699-1707. doi:10.4049/jimmunol.1200729

Barrow-McGee, R., Kishi, N., Joffre, C., Menard, L., Hervieu, A., Bakhouche, B. A., Noval, A. J., Mai, A., Guzman, C., Robbez-Masson, L. et al. (2016). Beta 1-integrin-c-Met cooperation reveals an inside-in survival signalling on autophagy-related endomembranes. *Nat. Commun.* **7**, 11942. doi:10.1038/ncomms11942

Benvenuti, S. and Comoglio, P. M. (2007). The MET receptor tyrosine kinase in invasion and metastasis. *J. Cell. Physiol.* **213**, 316-325. doi:10.1002/jcp.21183

Charest, P. G., Shen, Z., Lakoduk, A., Sasaki, A. T., Briggs, S. P. and Firtel, R. A. (2010). A Ras signaling complex controls the RasC-TORC2 pathway and directed cell migration. *Dev. Cell* **18**, 737-749. doi:10.1016/j.devcel.2010.03.017

Chernyavsky, A. I., Arredondo, J., Karlsson, E., Wessler, I. and Grando, S. A. (2005). The Ras/Raf-1/MEK1/ERK signaling pathway coupled to integrin expression mediates cholinergic regulation of keratinocyte directional migration. *J. Biol. Chem.* **280**, 39220-39228. doi:10.1074/jbc.M504407200

Courret, N., Darche, S., Sonigo, P., Milon, G., Buzoni-Gatel, D. and Tardieux, I. (2006). CD11c- and CD11b-expressing mouse leukocytes transport single Toxoplasma gondii tachyzoites to the brain. *Blood* **107**, 309-316. doi:10.1182/blood-2005-02-0666

Cox, A. D., Hisaka, M. M., Buss, J. E. and Der, C. J. (1992). Specific isoprenoid modification is required for function of normal, but not oncogenic, Ras protein. *Mol. Cell. Biol.* **12**, 2606-2615. doi:10.1128/MCB.12.6.2606

Cullen, P. J. and Lockyer, P. J. (2002). Integration of calcium and Ras signalling. *Nat. Rev. Mol. Cell Biol.* **3**, 339-348. doi:10.1038/nrm808

David, F. P., Rougemont, J. and Deplancke, B. (2017). GETPrime 2.0: gene- and transcript-specific qPCR primers for 13 species including polymorphisms. *Nucleic Acids Res.* **45**, 56-60. doi:10.1093/nar/gkw913

Dolmetsch, R. E., Pajvani, U., Fife, K., Spotts, J. M. and Greenberg, M. E. (2001). Signaling to the nucleus by an L-type calcium channel-calmodulin complex through the MAP kinase pathway. *Science* **294**, 333-339. doi:10.1126/science.1063395

Drewry, L. L., Jones, N. G., Wang, Q., Onken, M. D., Miller, M. J. and Sibley, L. D. (2019). The secreted kinase ROP17 promotes Toxoplasma gondii dissemination by hijacking monocyte tissue migration. *Nat. Microbiol.* **4**, 1951-1963. doi:10.1038/s41564-019-0504-8

Ebert, P. J. R., Cheung, J., Yang, Y., McNamara, E., Hong, R., Moskalenko, M., Gould, S. E., Maecker, H., Irving, B. A., Kim, J. M. et al. (2016). MAP kinase inhibition promotes T cell and anti-tumor activity in combination with PD-L1 checkpoint blockade. *Immunity* **44**, 609-621. doi:10.1016/j.immuni.2016.01.024

Eblen, S. T. (2018). Extracellular-regulated kinases: signaling from Ras to ERK substrates to control biological outcomes. *Adv. Cancer Res.* **138**, 99-142. doi:10.1016/bs.acr.2018.02.004

Fischer, O. M., Giordano, S., Comoglio, P. M. and Ullrich, A. (2004). Reactive oxygen species mediate Met receptor transactivation by G protein-coupled receptors and the epidermal growth factor receptor in human carcinoma cells. *J. Biol. Chem.* **279**, 28970-28978. doi:10.1074/jbc.M402508200

Fuks, J. M., Arrighi, R. B., Weidner, J. M., Kumar Mendu, S., Jin, Z., Wallin, R. P., Rethi, B., Birnir, B. and Barragan, A. (2012). GABAergic signaling is linked to a hypermigratory phenotype in dendritic cells infected by Toxoplasma gondii. *PLoS Pathog.* **8**, e1003051. doi:10.1371/journal.ppat.1003051

Giehl, K., Skripczynski, B., Mansard, A., Menke, A. and Gierschik, P. (2000). Growth factor-dependent activation of the Ras-Raf-MEK-MAPK pathway in the human pancreatic carcinoma cell line PANC-1 carrying activated K-ras: implications for cell proliferation and cell migration. *Oncogene* **19**, 2930-2942. doi:10.1038/sj.onc.1203612

Hartmann, G., Weidner, K. M., Schwarz, H. and Birchmeier, W. (1994). The motility signal of scatter factor/hepatocyte growth factor mediated through the receptor tyrosine kinase met requires intracellular action of Ras. *J. Biol. Chem.* **269**, 21936-21939.

Hui, A. Y., Meens, J. A., Schick, C., Organ, S. L., Qiao, H., Tremblay, E. A., Schaeffer, E., Uniyal, S., Chan, B. M. and Elliott, B. E. (2009). Src and FAK mediate cell-matrix adhesion-dependent activation of Met during transformation of breast epithelial cells. *J. Cell. Biochem.* **107**, 1168-1181. doi:10.1002/jcb.22219

Kanatani, S., Uhlén, P. and Barragan, A. (2015). Infection by Toxoplasma gondii induces amoeboid-like migration of dendritic cells in a three-dimensional collagen matrix. *PLoS ONE* **10**, e0139104. doi:10.1371/journal.pone.0139104

Kanatani, S., Fuks, J. M., Olafsson, E. B., Westermark, L., Chambers, B., Varas-Godoy, M., Uhlén, P. and Barragan, A. (2017). Voltage-dependent calcium channel signaling mediates GABAA receptor-induced migratory activation of dendritic cells infected by Toxoplasma gondii. *PLoS Pathog.* **13**, e1006739. doi:10.1371/journal.ppat.1006739

Kaufmann, R., Oettel, C., Horn, A., Halbhuber, K. J., Eitner, A., Krieg, R., Katenkamp, K., Henklein, P., Westermann, M., Bohmer, F. D. et al. (2009). Met receptor tyrosine kinase transactivation is involved in proteinase-activated receptor-2-mediated hepatocellular carcinoma cell invasion. *Carcinogenesis* **30**, 1487-1496. doi:10.1093/carcin/bgp153

Kim, L., Butcher, B. A., Lee, C. W., Uematsu, S., Akira, S. and Denkers, E. Y. (2006). Toxoplasma gondii genotype determines MyD88-dependent signaling in infected macrophages. *J. Immunol.* **177**, 2584-2591. doi:10.4049/jimmunol.177.4.2584

Kotturi, M. F., Carlow, D. A., Lee, J. C., Ziltener, H. J. and Jefferies, W. A. (2003). Identification and functional characterization of voltage-dependent calcium channels in T lymphocytes. *J. Biol. Chem.* **278**, 46949-46960. doi:10.1074/jbc.M309268200

Lambert, H., Hitziger, N., Dellacasa, I., Svensson, M. and Barragan, A. (2006). Induction of dendritic cell migration upon Toxoplasma gondii infection potentiates parasite dissemination. *Cell. Microbiol.* **8**, 1611-1623. doi:10.1111/j.1462-5822.2006.00735.x

Lambert, H., Vutova, P. P., Adams, W. C., Lore, K. and Barragan, A. (2009). The Toxoplasma gondii-shuttling function of dendritic cells is linked to the parasite genotype. *Infect. Immun.* **77**, 1679-1688. doi:10.1128/IAI.01289-08

Lambert, A. W., Pattabiraman, D. R. and Weinberg, R. A. (2017). Emerging biological principles of metastasis. *Cell* **168**, 670-691. doi:10.1016/j.cell.2016.11.037

Lemmon, M. A. and Schlessinger, J. (2010). Cell signaling by receptor tyrosine kinases. *Cell* **141**, 1117-1134. doi:10.1016/j.cell.2010.06.011

Li, Y., Lin, J. L., Reiter, R. S., Daniels, K., Soll, D. R. and Lin, J. J. (2004). Caldesmon mutant defective in Ca(2+)-calmodulin binding interferes with assembly of stress fibers and affects cell morphology, growth and motility. *J. Cell Sci.* **117**, 3593-3604. doi:10.1242/jcs.01216

Liu, C. H., Fan, Y.-T., Dias, A., Esper, L., Corn, R. A., Bafica, A., Machado, F. S. and Aliberti, J. (2006). Cutting edge: dendritic cells are essential for in vivo IL-12 production and development of resistance against Toxoplasma gondii infection in mice. *J. Immunol.* **177**, 31-35. doi:10.4049/jimmunol.177.1.31

Lundberg, M. S., Curto, K. A., Bilato, C., Monticone, R. E. and Crow, M. T. (1998). Regulation of vascular smooth muscle migration by mitogen-activated protein kinase and calcium/calmodulin-dependent protein kinase II signaling pathways. *J. Mol. Cell. Cardiol.* **30**, 2377-2389. doi:10.1006/jmcc.1998.0795

Mitra, A. K., Sawada, K., Tiwari, P., Mui, K., Gwin, K. and Lengyel, E. (2011). Ligand-independent activation of c-Met by fibronectin and $alpha_5beta_1$-integrin regulates ovarian cancer invasion and metastasis. *Oncogene* **30**, 1566-1576. doi:10.1038/onc.2010.532

Montoya, J. G. and Liesenfeld, O. (2004). Toxoplasmosis. *Lancet* **363**, 1965-1976. doi:10.1016/S0140-6736(04)16412-X

Muniz-Feliciano, L., Van Grol, J., Portillo, J.-A. C., Liew, L., Liu, B., Carlin, C. R., Carruthers, V. B., Matthews, S. and Subauste, C. S. (2013). Toxoplasma gondii-induced activation of EGFR prevents autophagy protein-mediated killing of the parasite. *PLoS Pathog.* **9**, e1003809. doi:10.1371/journal.ppat.1003809

Nordgaard, C., Doll, S., Matos, A., Hoeberg, M., Kazi, J. U., Friis, S., Stenvang, J., Ronnstrand, L., Mann, M. and Moreira, J. M. A. (2019). Metallopeptidase Inhibitor 1 (TIMP-1) promotes receptor tyrosine kinase c-Kit signaling in colorectal cancer. *Mol. Oncol.* **13**, 2646-2662. doi:10.1002/1878-0261.12575

Ólafsson, E. B., Varas-Godoy, M. and Barragan, A. (2018). Toxoplasma gondii infection shifts dendritic cells into an amoeboid rapid migration mode encompassing podosome dissolution, secretion of TIMP-1, and reduced proteolysis of extracellular matrix. *Cell. Microbiol.* **20**, 10.1111/cmi.12808. doi:10.1111/cmi.12808

Ólafsson, E. B., Ross, E. C., Varas-Godoy, M. and Barragan, A. (2019). TIMP-1 promotes hypermigration of Toxoplasma-infected primary dendritic cells via CD63-ITGB1-FAK signaling. *J. Cell Sci.* **132**, jcs225193. doi:10.1242/jcs.225193

Pappas, G., Roussos, N. and Falagas, M. E. (2009). Toxoplasmosis snapshots: global status of Toxoplasma gondii seroprevalence and implications for pregnancy and congenital toxoplasmosis. *Int. J. Parasitol.* **39**, 1385-1394. doi:10.1016/j.ijpara.2009.04.003

Riegel, K., Schlöder, J., Sobczak, M., Jonuleit, H., Thiede, B., Schild, H. and Rajalingam, K. (2019). RAF kinases are stabilized and required for dendritic cell differentiation and function. *Cell Death Differ.* doi:10.1038/s41418-019-0416-4

Rosen, L. B., Ginty, D. D., Weber, M. J. and Greenberg, M. E. (1994). Membrane depolarization and calcium influx stimulate MEK and MAP kinase via activation of Ras. *Neuron* **12**, 1207-1221. doi:10.1016/0896-6273(94)90438-3

Sangare, L. O., Olafsson, E. B., Wang, Y., Yang, N., Julien, L., Camejo, A., Pesavento, P., Sidik, S. M., Lourido, S., Barragan, A. et al. (2019). In vivo CRISPR screen identifies TgWIP as a Toxoplasma modulator of dendritic cell migration. *Cell Host Microbe* **26**, 478-492.e8. doi:10.1016/j.chom.2019.09.008

Sasaki, A. T., Chun, C., Takeda, K. and Firtel, R. A. (2004). Localized Ras signaling at the leading edge regulates PI3K, cell polarity, and directional cell movement. *J. Cell Biol.* **167**, 505-518. doi:10.1083/jcb.200406177

Scheele, J. S., Marks, R. E. and Boss, G. R. (2007). Signaling by small GTPases in the immune system. *Immunol. Rev.* **218**, 92-101. doi:10.1111/j.1600-065X.2007.00530.x

Schlaepfer, D. D., Hanks, S. K., Hunter, T. and van der Geer, P. (1994). Integrin-mediated signal transduction linked to Ras pathway by GRB2 binding to focal adhesion kinase. *Nature* **372**, 786-791. doi:10.1038/372786a0

Schwanhausser, B., Busse, D., Li, N., Dittmar, G., Schuchhardt, J., Wolf, J., Chen, W. and Selbach, M. (2011). Global quantification of mammalian gene expression control. *Nature* **473**, 337-342. doi:10.1038/nature10098

Shi, S., Zhang, J., Liu, M., Dong, H. and Li, N. (2019). Ras-ERK signalling represses H1.4 phosphorylation at serine 36 to promote non-small-cell lung carcinoma cells growth and migration. *Artif. Cells Nanomed. Biotechnol.* **47**, 2343-2351. doi:10.1080/21691401.2019.1624558

Sibley, L. D. (2004). Intracellular parasite invasion strategies. *Science* **304**, 248-253. doi:10.1126/science.1094717

Stupack, D. G., Cho, S. Y. and Klemke, R. L. (2000). Molecular signaling mechanisms of cell migration and invasion. *Immunol. Res.* **21**, 83-88. doi:10.1385/IR:21:2-3:83

ten Hoeve, A. L., Hakimi, M.-A. and Barragan, A. (2019). Sustained Egr-1 response via p38 MAP kinase signaling modulates early immune responses of dendritic cells parasitized by Toxoplasma gondii. *Front. Cell Infect. Microbiol.* **9**, 349. doi:10.3389/fcimb.2019.00349

Tracey, A., Martin, T. A., Sanders, A. J., Lane, J. and Jiang, W. G. (2013). *Cancer Invasion and Metastasis: Molecular and Cellular Perspective*. Austin, TX: Landes Bioscience.

Vaillant, A. R., Mazzoni, I., Tudan, C., Boudreau, M., Kaplan, D. R. and Miller, F. D. (1999). Depolarization and neurotrophins converge on the phosphatidylinositol 3-kinase-Akt pathway to synergistically regulate neuronal survival. *J. Cell Biol.* **146**, 955-966. doi:10.1083/jcb.146.5.955

Vela, J., Pérez-Millán, M. I., Becu-Villalobos, D. and Díaz-Torga, G. (2007). Different kinases regulate activation of voltage-dependent calcium channels by depolarization in GH3 cells. *Am. J. Physiol. Cell Physiol.* **293**, C951-C959. doi:10.1152/ajpcell.00429.2006

Viala, E. and Pouysségur, J. (2004). Regulation of tumor cell motility by ERK mitogen-activated protein kinases. *Ann. N. Y. Acad. Sci.* **1030**, 208-218. doi:10.1196/annals.1329.027

Volinsky, N. and Kholodenko, B. N. (2013). Complexity of receptor tyrosine kinase signal processing. *Cold Spring Harb. Perspect. Biol.* **5**, a009043. doi:10.1101/cshperspect.a009043

von Kriegsheim, A., Baiocchi, D., Birtwistle, M., Sumpton, D., Bienvenut, W., Morrice, N., Yamada, K., Lamond, A., Kalna, G., Orton, R. et al. (2009). Cell fate decisions are specified by the dynamic ERK interactome. *Nat. Cell Biol.* **11**, 1458-1464. doi:10.1038/ncb1994

Wang, D., Li, Z., Messing, E. M. and Wu, G. (2002). Activation of Ras/Erk pathway by a novel MET-interacting protein RanBPM. *J. Biol. Chem.* **277**, 36216-36222. doi:10.1074/jbc.M205111200

Webb, C. P., Taylor, G. A., Jeffers, M., Fiscella, M., Oskarsson, M., Resau, J. H. and Vande Woude, G. F. (1998). Evidence for a role of Met-HGF/SF during Ras-mediated tumorigenesis/metastasis. *Oncogene* **17**, 2019-2025. doi:10.1038/sj.onc.1202135

Weidner, J. M. and Barragan, A. (2014). Tightly regulated migratory subversion of immune cells promotes the dissemination of Toxoplasma gondii. *Int. J. Parasitol.* **44**, 85-90. doi:10.1016/j.ijpara.2013.09.006

Weidner, J. M., Kanatani, S., Hernández-Castañeda, M. A., Fuks, J. M., Rethi, B., Wallin, R. P. and Barragan, A. (2013). Rapid cytoskeleton remodelling in dendritic cells following invasion by Toxoplasma gondii coincides with the onset of a hypermigratory phenotype. *Cell. Microbiol.* **15**, 1735-1752. doi:10.1111/cmi.12145

Weidner, J. M., Kanatani, S., Uchtenhagen, H., Varas-Godoy, M., Schulte, T., Engelberg, K., Gubbels, M.-J., Sun, H. S., Harrison, R. E., Achour, A. et al. (2016). Migratory activation of parasitized dendritic cells by the protozoan Toxoplasma gondii 14-3-3 protein. *Cell. Microbiol.* **18**, 1537-1550. doi:10.1111/cmi.12595

Zhou, Y., Wong, C.-O., Cho, K.-J., van der Hoeven, D., Liang, H., Thakur, D. P., Luo, J., Babic, M., Zinsmaier, K. E., Zhu, M. X. et al. (2015). Membrane potential modulates plasma membrane phospholipid dynamics and K-Ras signaling. *Science* **349**, 873-876. doi:10.1126/science.aaa5619

Table S1. Sequences of shRNAs

Target	Sequence (5′ to 3′)
shLuc	Fd:TGTTCTCCGAACGTGTCACGTTTCAAGAGAACGTGACACGTTCGGAGAACTTTTTTC Rv:CGAGAAAAAAGTTCTCCGAACGTGTCACGTTCTCTTGAAACGTGACACGTTCGGAGAACA
shMet	Fd:TGGTCATAGGAAGAGGGCATTTTTTCAAGAGAAAAATGCCCTCTTCCTATGACCTTTTTTC Rv:TCGAGAAAAAAGGTCATAGGAAGAGGGCATTTTTCTCTTGAAAAAATGCCCTCTTCCTATGACCA
shErk1	Fd:TGGGCTACACCAAATCCATCGACATTCAAGAGATGTCGATGGATTTGGTGTAGCCCTTTTTTC Rv:TCGAGAAAAAAGGGCTACACCAAATCCATCGACATCTCTTGAATGTCGATGGATTTGGTGTAGCCCA
shErk2	Fd:TGGGAAGATCTGAATTGTATAATAATTCAAGAGATTATTATACAATTCAGATCTTCCCTTTTTTC Rv:TCGAGAAAAAAGGGAAGATCTGAATTGTATAATAATCTCTTGAATTATTATACAATTCAGATCTTCCCA

Table S2. PCR primers used to amplify met, hgf, erk1 and erk2

Target	Primer pair sequence (5´to 3´)	Tm (°C)
met	Fd: AGAGTGGAAGCAAGCAGTCTC	59
	Rv: ACTCTTGCGTCATAGCGAACT	58
hgf	Fd: AGGCAGCTATAAAGGGACGG	59
	Rv: ACCGCGATAGCTGTGTTCAT	58
erk1 (mapk3)	Fd: CACTGGCTTTCTGACGGAGT	59
	Rv: CCGGTTGGAGAGCATCTCAG	60
erk2 (mapk1)	Fd: TCAGTTTGTCCCCTTCCATTGAT	58
	Rv: AGTCCACTCCCACAATGCAC	59

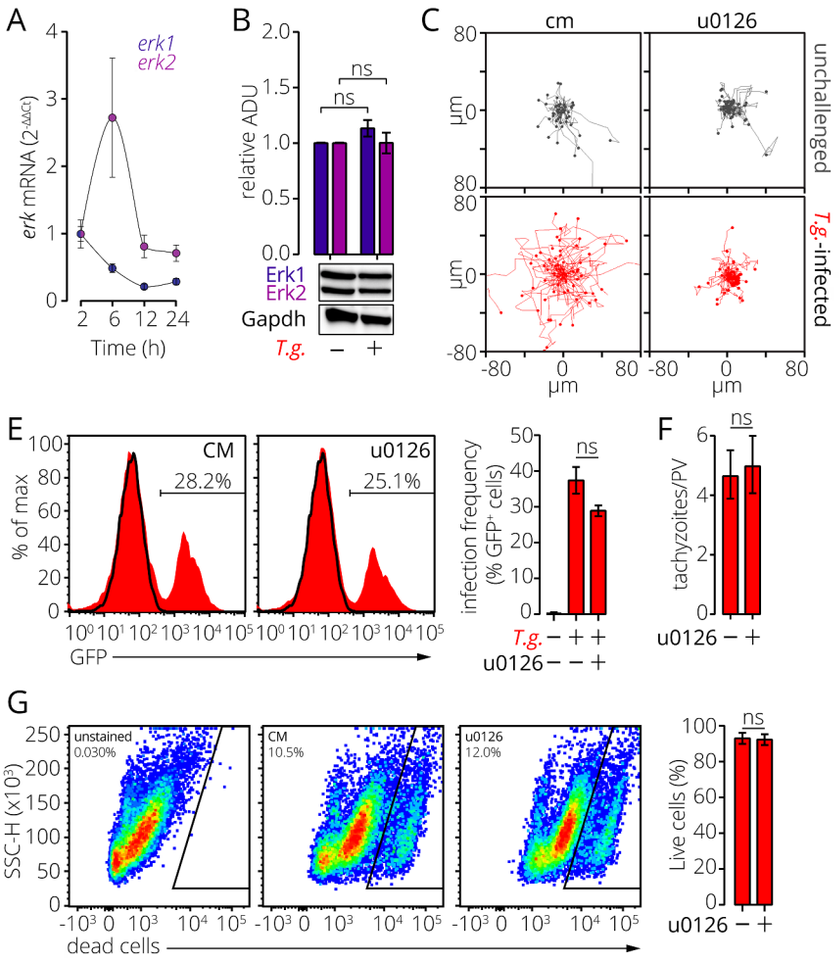

Figure S1. Expression of Erk1/2 mRNA and total protein by *T. gondii*-challenged DCs and impact of Erk inhibition on DC motility, viability and *T. gondii* infection frequency.

A. Fold change in *erk1* and *erk2* mRNA expression in *T. gondii*-challenged DCs at 2, 6, 12 and 24 h post-infection (hpi). Graph shows mean expression (± SEM) related to gapdh ($2^{-\Delta Ct}$) and unchallenged DCs ($2^{-\Delta\Delta Ct}$, n=3 independent experiments).

B. Total Erk protein expression in unchallenged and *T. gondii*-challenged DCs at 6 hpi. Bar graph shows mean (± SEM) Erk total protein related to Gapdh. Expression of unchallenged DCs was set to 1. Images show representative blots used for quantification from 1 experiment (n=4 biological replicates from independent blots).

C. Representative motility plots of unchallenged and *T. gondii*-infected DCs embedded in collagen ± u0126 (10 µM). Plots are representative of 3 independent experiments.

D. Representative dot plots of flow cytometry analyses of *T. gondii* infection frequency. Dot plots show gating of cells (FSC-A/ SSC-A) and single cells (FSC-A/ FSC-H).

E. *T. gondii* infection frequencies of DCs cultured in complete medium (CM) ± u0126 (10 µM). Histograms show gates used to define *T. gondii* (GFP^+)-infected cells in unchallenged (black line) and *T. gondii*-challenged (red fill) DCs and are representative of 3 experiments. Bar graph shows mean percentage (± SEM) of GFP^+ cells (n=3).

F. Replication analysis of *T. gondii* tachyzoites in HFFs incubated in CM ± u0126 (10 µM). Both conditions were treated with vehicle (DMSO). Bar graph shows mean number of tachyzoites per PV (± SD) from 3 independent experiments (n=3).

G. Live/dead analysis of *T. gondii*-challenged DCs in CM ± u0126 (10µM) 5 hpi. Both conditions were treated with vehicle (DMSO). Dot plots show gate used to define dead cells (SSC-H/ Live dead-BV421). The percentage of dead cells for each representative plot is shown. Bar graph shows mean percentage (± SEM) of live cells from three independent experiments (n=3).

Ns indicates non-significant difference: One-way ANOVA, Tukey's HSD post-hoc test (B and E); Unpaired t-test (F and G).

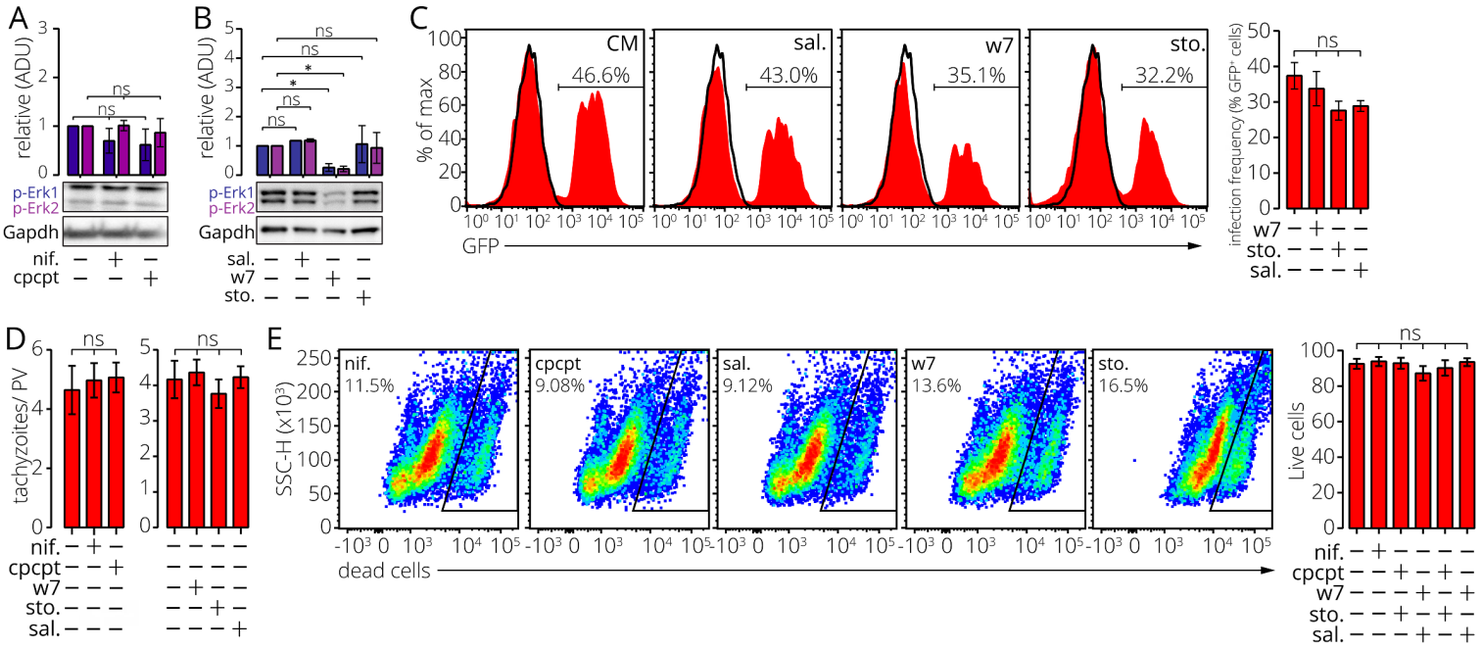

Figure S2. Erk phosphorylation in unchallenged DCs and *T. gondii* infection frequency, replication and DC viability in presence of VGCC, CaM, CaMkII and Ras inhibitors.

A. Erk phosphorylation in unchallenged DCs ± nifedipine (50 µM) or cpcpt (10 µM) treatment 2 hpi. Bar graph shows mean (± SEM) phosphorylated Erk1 and Erk2 protein related to Gapdh. Expression of unchallenged DCs was set to 1. Images show representative blots used for quantification from 1 experiment (n=3 biological replicates from independent blots).

B. Erk phosphorylation in unchallenged DCs ± salirasib (100 µM), w7 (25 µM) or sto-609 (sto., 50 µM) treatment 2 hpi. Bar graph shows mean (± SEM) phosphorylated Erk1 and Erk2 protein related to Gapdh. Expression of unchallenged DCs was set to 1. Images show representative blots used for quantification from 1 experiment (n=3 biological replicates from independent blots).

C. *T. gondii* infection frequency of DCs cultured in CM ± w7 (25 µM), sto-609 (sto., 50 µM) or salirasib (sal.,100 µM). Histograms show gates used to define *T. gondii* (GFP^+)-infected cells in unchallenged (black line) and *T. gondii*-challenged (red fill) DCs and are representative of 3 experiments. Bar graph shows mean percentage (± SEM) of GFP^+ cells (n=3).

D. Replication analysis of *T. gondii* tachyzoites in HFFs incubated in CM ± nifedipine (50 µM), cpcpt (10 µM), w7 (25 µM), sto-609 (sto., 50 µM) or salirasib (sal.,100 µM). All conditions were treated with vehicle (DMSO). Bar graph shows mean number of tachyzoites per PV (± SD) from 3 independent experiments (n=3).

E. Live/dead analysis of *T. gondii*-challenged DCs ± nifedipine (nif., 50 µM), cpcpt (10 µM), salirasib (sal., 100 µM), w7 (25 µM) or sto-609 (sto.,50 µM) 5 hpi. All conditions were treated with vehicle (DMSO). Dot plots show gate used to define dead cells (SSC-H/ Live dead-BV421). The percentage of dead cells for each representative plot is shown. Bar graph shows mean percentage (± SEM) of live cells from three independent experiments (n=3).

Asterisks (*) indicate significant difference, ns: non-significant difference: One-way ANOVA, Tukey's HSD post-hoc test (A, C, D and E), Unpaired t-test (B).

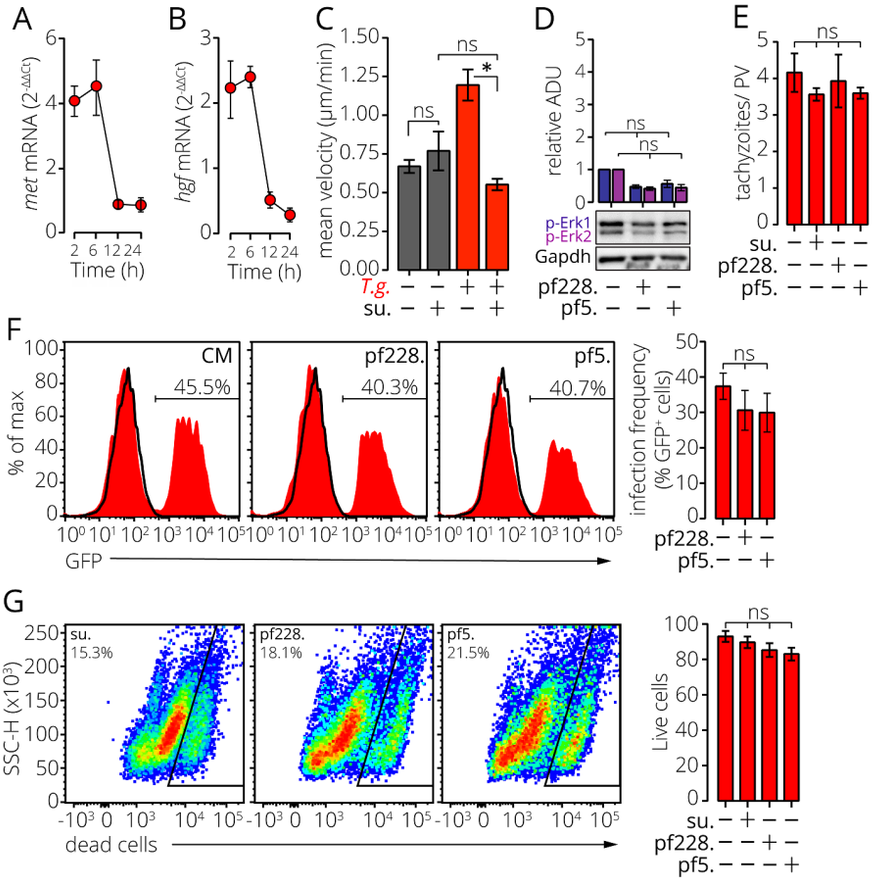

Figure S3. *Met* and *hgf* expression in *T. gondii*-challenged DCs and impact of tyrosine kinase inhibition on Erk phosphorylation in unchallenged DCs, *T. gondii* infection frequency, replication and DC viability.

A. Fold change Met mRNA expression in *T. gondii*-challenged DCs at 2, 6, 12 and 24 hpi. Bar graph shows mean expression (± SEM) related to gapdh (2-ΔCt) and unchallenged DCs ($2^{-\Delta\Delta Ct}$, n=3 independent experiments).

B. Fold change Hgf mRNA expression in T. gondii-challenged DCs at 2, 6, 12 and 24 hpi. Bar graph shows mean expression (± SEM) related to gapdh (2-ΔCt) and unchallenged DCs ($2^{-\Delta\Delta Ct}$, n=3 independent experiments).

C. Bar graph shows mean velocity (± SEM) of unchallenged and *T. gondii*-infected DCs (*T.g.*) embedded in collagen ± su11274 (10 µM) (n=3 independent experiments).

D. Erk phosphorylation in unchallenged DCs ± pf228 (10 µM) or pf5 (10 µM) treatment 2 hpi. Bar graph shows mean (± SEM) phosphorylated Erk1 and Erk2 protein related to Gapdh. Expression of unchallenged DCs was set to 1. Images show representative blots used for quantification from 1 experiment (n=3 biological replicates from independent blots).

E. Replication analysis of *T. gondii* tachyzoites in HFFs incubated in CM± su11274 (su.,10 µM), pf228 (10 µM) or pf5 (10 µM). All conditions were treated with vehicle (DMSO). Bar graph shows mean number of tachyzoites per PV (± SD) from 3 independent experiments (n=3).

F. *T. gondii* infection frequency of DCs cultured in cm ± pf228 (10 µM) or pf5 (10 µM). Histograms show gates used to define *T. gondii* (GFP^+)-infected cells in unchallenged (black line) and *T. gondii*-challenged (red fill) DCs and are representative of 3 experiments. Bar graph shows mean percentage (± SEM) of GFP^+ cells (n=3).

G. Live/dead analysis of *T. gondii*-challenged DCs ± su11274 (su., 10 µM), pf228 (10 µM) or pf5 (sal., 10 µM) 5 hpi. All conditions were treated with vehicle (DMSO). Dot plots show gate used to define dead cells (SSC-A/ Live dead-BV421). The percentage of dead cells for each representative plot is shown. Bar graph shows mean percentage (± SEM) of live cells from three independent experiments (n=3).

Ns: non-significant difference: One-way ANOVA, Tukey's HSD post-hoc test (C and E-G) or Holm-Sidak's multiple comparisons test (D).

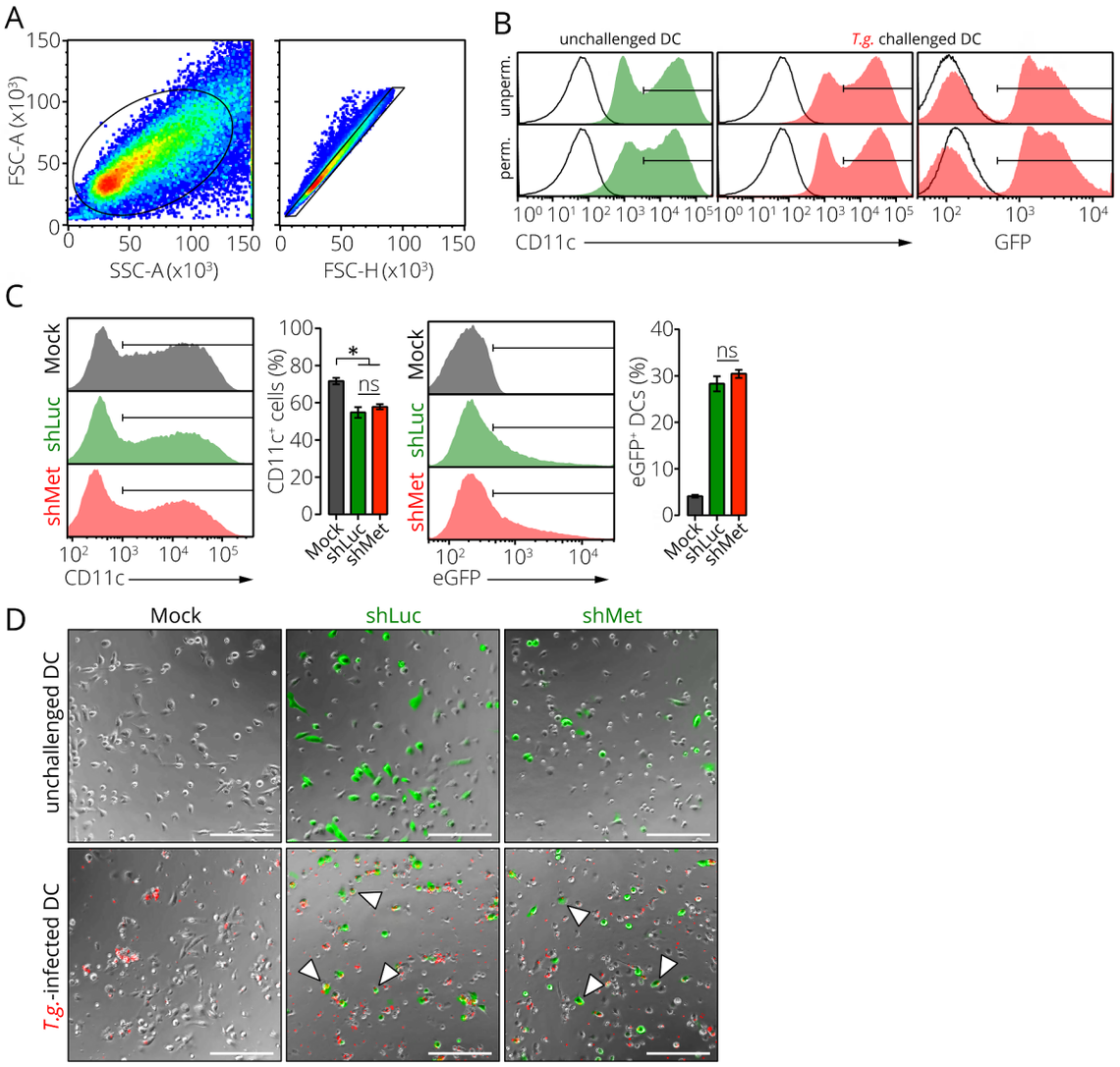

Figure S4. Characterizations of Met expression and gene silencing of *met* for motility analyses.
A. Representative dot plots used in flow cytometry analyses of Met protein expression. Dot plots show gating of cells (FSC-A/ SSC-A) and single cells (FSC-A/ FSC-H). Plots are representative of 3 experiments.
B. Histograms show gates used to define CD11c⁺ cells (left) and *T. gondii*-GFP⁺ infected cells (GFP; right) in unchallenged (green) and *T. gondii*-challenged (red) cells used in Met protein analyses. Both unpermeabilized (unperm.) and permeabilized (perm.) populations were analyzed. Black lines represent unstained control for CD11c and unchallenged control for *T.g.* challenged DCs. Histograms are representative of 3 experiments.
C. Histograms show gates used to define CD11c⁺ cells (left panel) and eGFP⁺ cells (right panel) in mock-treated (Mock, grey), shLuc (green) and shMet (red) -transduced cells. Bar graphs shows mean percentage (± SEM) of CD11c⁺ (left) and GFP⁺ (right) cells for each condition (n=3).
D. Representative micrographs of mock-treated DCs (Mock) and eGFP-expressing DCs transduced with lentiviral vectors targeting met mRNA (shMet) or a non-expressed target (shLuc) embedded in collagen ± RFP-expressing *T. gondii* tachyzoites. Arrowheads indicate *T. gondii*-infected cells expressing an eGFP-reporter assessed in the assay. Scale bars: 200 µm. Micrographs are representative of 3 independent experiments.
Asterisk (*) indicates significant difference, ns: non-significant difference: One-way ANOVA, Tukey's HSD post-hoc test (C)